Annales Societatis Geologorum Poloniae (2019), vol. 89: 47–81. doi: https://doi.org/10.14241/asgp.2019.07

THE IMPACT OF FOSSILS ON DIAGENETICALLY CONTROLLED RESERVOIR QUALITY: THE ZECHSTEIN BROŃSKO REEF (UPPER PERMIAN, W POLAND)

Adam FHEED

AGH University of Science and Technology, Faculty of Geology, Geophysics and Environmental Protection, Department of Fossil Fuels, Mickiewicza 30; 30-059 Kraków, Poland; e-mail: fheed@agh.edu.pl

Fheed, A., 2019. The impact of fossils on diagenetically controlled reservoir quality: the Zechstein Brońsko Reef (Upper Permian, W Poland). *Annales Societatis Geologorum Poloniae*, 89: 47–81.

Abstract: Although the sedimentation and diagenesis of the Polish Zechstein Limestone strata (Ca1, Permian) already have been investigated, relatively little has been done to resolve their petrophysical potential. Therefore, the gap between sedimentological and petrophysical studies was bridged through an integrated analysis of geological and geophysical data. The results of core description, polarized-light microscopy, well log interpretations and laboratory measurements on core samples were combined with previously published nuclear magnetic resonance (NMR) and X-ray microtomography (μCT) data, especially helpful in the recognition of pore geometry. The Ca1 strata of the Brońsko-1 and Brońsko-2 wells, located on the Zechstein Brońsko Reef (West Poland), were studied to determine the influence of fossils on porosity and permeability. It was concluded that greater diversification of the original biota led to an increase in porosity and variation in pore geometry. While encrusting organisms such as foraminifers promoted the development of channel and fracture porosity, the dissolution of the primarily aragonitic bivalve and gastropod shells and the shells of terebratulid brachiopods often gave rise to the formation of cavernous and mouldic porosity. The channels appear to be most common in the bryozoan-foraminifer biofacies, representing a shallowing of the depositional environment. Caverns, in turn, corresponded to the organisms of the brachiopod-bryozoan and the lightly karstified bivalve-gastropod biofacies, both of which probably experienced the influence of sabkha conditions, leading to a general decrease in porosity. The bryozoan zoecia tended to enhance both primary intraparticle voids, and after their dissolution, secondary intraparticle pores, which showed limited connectivity in the high-energy *Acanthocladia* biofacies, where considerable fragmentation of fossils took place, hence decreasing the permeability. Anhydrite cementation was found to be the most pronounced factor controlling porosity destruction, while dolomitization enhanced it significantly, especially for the stromatolitic biofacies, where small, unconnected vugs were formed owing to this process. The permeability is typically below 100 mD, and this is caused by the rich diagenetic history of the reef, that recorded marine, sabkha-related and burial cementation, now represented by the different fabrics of anhydrite, calcite, and dolomite.

Key words: Carbonates, dissolution channels, diagenesis, fossils, porosity.

Manuscript received 22 November 2018, accepted 11 June 2019

INTRODUCTION

In considerations of the quality of a hydrocarbon reservoir, the main goal is to find the most porous and permeable intervals, ensuring the retention and migration of fluids, which presents a challenge for highly altered, fossiliferous carbonate reservoirs (cf. Stanley, 2001; Mazzullo, 2004; Ahr *et al*., 2005; Flügel, 2010). In such cases, sedimentological analysis might help an understanding of the relations between water depth and energy, fossils, and the resulting geometry of pores impacting the permeability.

The Zechstein Limestone (Ca1) reefs are known to occur in Western and Central Europe owing to a rapid inundation of the Southern Permian Basin (SPBA) during Zechstein (late Permian) times (Doornenbal *et al*., 2010; Kiersnowski *et al*., 2010). Bryozoan-rich reefs were noted in England (e.g., Smith, 1995), the Netherlands (e.g., Van der Baan, 1990), Denmark (e.g., Clark, 1986), Germany (e.g., Füchtbauer, 1964; Becker and Bechstädt, 2006; Paul, 2010) and Poland (e.g., Dyjaczyński *et al*., 1997, 2001; Raczyński, 2000; Mikołajewski *et al*., 2009; T. M. Peryt *et al*., 2012, 2016; Fheed *et al*., 2015; Raczyński *et al*., 2017). In Europe, the Ca1 reefs developed within the deep basin, owing to the existence of tectonically uplifted

horsts (e.g., Geluk, 2000; Kiersnowski *et al*., 2010), gypsum banks, and other elements that reduced the distance to sea-level (see Clark, 1986; Van der Baan, 1990). In Poland, a pre-Zechstein horst – the Wolsztyn Ridge – appeared to influence the growth and development of the reefs most significantly (Kiersnowski *et al*., 2010). Among them, the Brońsko Reef is the largest. It once contained significant gas reserves (Mikołajewski *et al*. 2009) and today might be considered for the underground storage of gas. As a result of many relative sea-level fluctuations and subsidence, the reef was exposed to various diagenetic and sedimentary processes. In places, it carries the signs of successive phases of meteoric dissolution, the episodic appearances of sabkha conditions, and a wealth of marine cements. Such processes were also typical for other Ca1 SPBA carbonates (T. M. Peryt, 1984; Kaldi, 1986; Hollingworth and Tucker, 1987; Van der Baan, 1990; Weidlich, 2002; Becker and Bechstädt, 2006; Reijers, 2012). Therefore, it is assumed that the present variability of pore geometries in the Brońsko Reef was governed by former biota, the dissolution and alteration of which are considered in this article.

The Polish Ca1, although thoroughly understood in terms of sedimentation (Raczyński, 2000; Dyjaczyński *et al*., 2001; T. M. Peryt *et al*., 2012; T. M. Peryt *et al*. 2016; Raczyński *et al*., 2017) and diagenesis (T. M. Peryt, 1984; Jasionowski *et al*., 2000; Jasionowski *et al*., 2014; Fheed *et al*., 2015), is still poorly elaborated in petrophysical terms, including the examination of pore geometry. In particular, little has been done to define the geometry of pores and their modes of origin. It is noteworthy that such approaches were taken only by Mikołajewski *et al*. (2009) with reference to the porosity and permeability of the Brońsko Reef and by Fheed *et al*. (2015), who added some sedimentological background to the observations on diagenesis for an isolated part of the Wielichowo Reef.

Unlike the situation existing since the early eighties in Western Europe, where the integration of sedimentological and petrophysical data has become a standard approach (see Clark, 1986; Frykman *et al*., 1990), the Polish Ca1 still awaits further multidisciplinary investigation. For instance, Clark (1986) characterized specific sedimentation zones, including reef, platform-edge and slope in the light of their

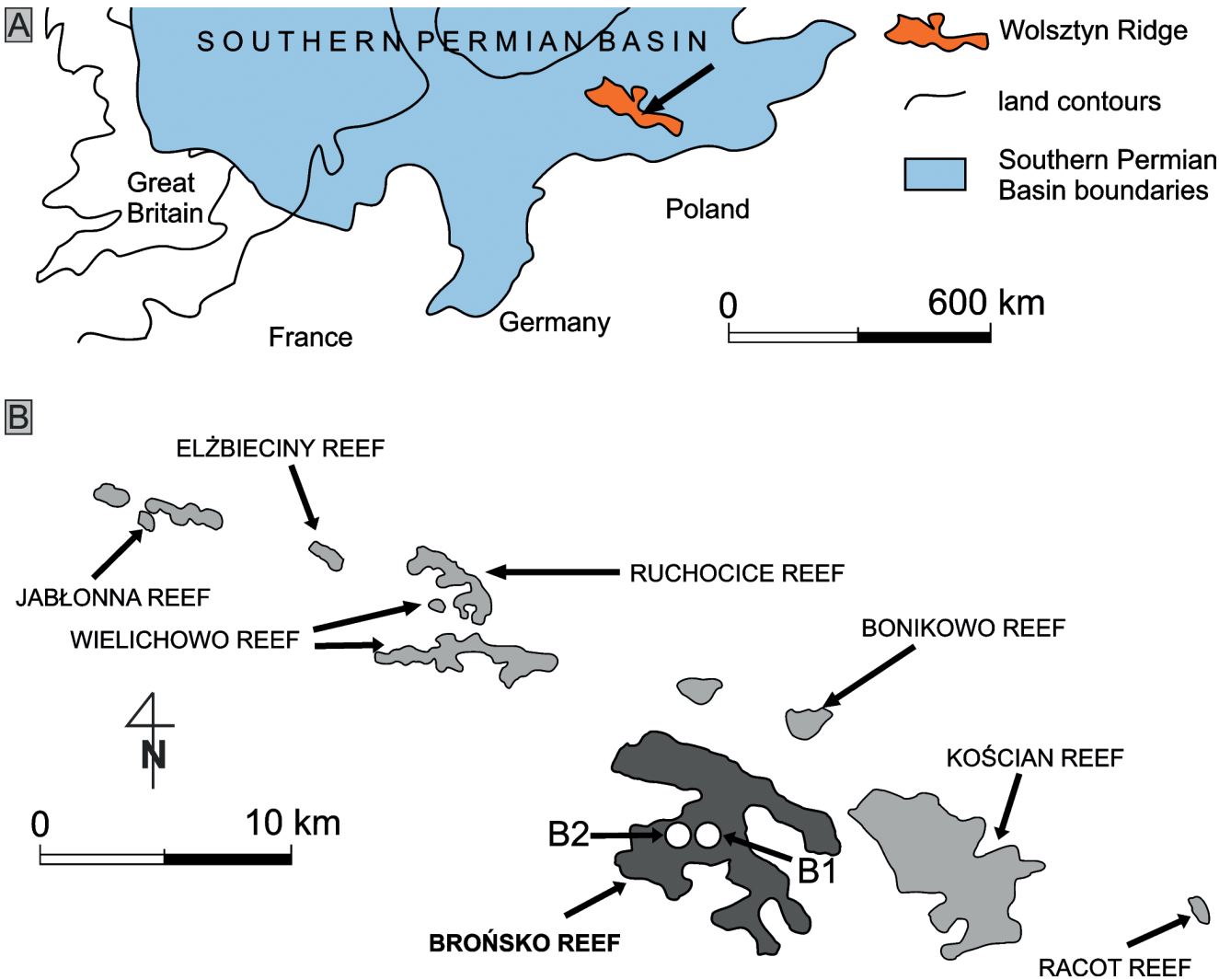

Fig. 1. Location of the study area. **A.** Geological setting on the background of the Southern Permian Basin (SPBA) and current land contours after Smith (1980). Location of the Brońsko Reef is arrowed on the Wolsztyn Ridge. **B.** Spatial distribution of the Wolsztyn Ridge reefs after Wilk (2008, Geofizyka Toruń, unpubl., modified) and Tomaszewska *et al*. (2008, PGNiG SA, unpubl.), reproduced from Fheed *et al*. (2015). North direction is arrowed. The locations of the Brońsko-1 (B1) and Brońsko-2 (B2) wells are shown.

petrophysical quality, thus facilitating hydrocarbon exploration within the Danish SPBA. Kaldi (1986) and Van der Baan (1990) went a step further by offering a comprehensive study of diagenetic alterations and related petrophysical features noted within the lagoon, oolite shoal and open marine shelf for the English and Dutch Zechstein sequences, respectively. Yet a different approach was demonstrated by Frykman *et al*. (1990), who brought together well logging, laboratory measurements and field observations.

This paper was designed to bridge the gap between sedimentological analyses and porosity/permeability assessment, regarding the Polish Ca1 strata, including well log and laboratory data interpretation, core description and microscope analyses. The author has chosen to focus on vertical variation of sedimentary conditions and their impact on porosity evolution, since it is the first step in spatial assessment of the influence of fossils on porosity-permeability relations. Five biofacies were characterized with reference to reservoir quality, including pore type, distribution and origin assessment, thus giving an idea of the influence of sedimentation on the parameters of a reservoir.

GEOLOGICAL SETTING

Two wells penetrating the central parts of the Brońsko Reef were studied (Fig. 1). These are the Brońsko-1 and Brońsko-2 wells, the latter being of lesser interest, so far. According to 3D seismic studies, both wells penetrate the reef facies (Dyjaczyński *et al.*, 2001). They occur on the Wolsztyn Ridge and are divided by the distance of roughly 1 km (Fig. 1B). The Brońsko Reef exhibits variable thickness, ranging between 19–91 m, and covers a total area of approximately 28.5 km^2 (Mikołajewski *et al*., 2009; Kiersnowski *et al*., 2010). In the present study, the thickness of the Ca1 reaches 53 m and only 19 m in the Brońsko-1 and Brońsko-2 wells, respectively (Figs 2, 3). Consequently, the Brońsko-2 well shows fewer biofacies and less complex assemblages of fossils.

The two well records examined are represented by various fossils, including bryozoans, brachiopods, bivalves, foraminifers, crinoids, gastropods and ostracods (cf. Raczyński, 2000; Kiersnowski *et al*., 2010; Raczyński *et al*., 2017). Red algae typically are restricted to the stromatolitic biofacies, and are much less common than in some other Ca1 reefs (see Raczyński *et al*., 2017). Both diagenetic and sedimentological processes were highly diversified.

MATERIAL AND METHODS

Core description and microscope research

Core slabs from the Brońsko-1 and Brońsko-2 wells (Fig. 1B) were examined. In total, roughly 70 m of drill cores were analysed, with an emphasis on fossil identification and the recognition of porosity types. On the basis of core descriptions, over 45 thin sections were prepared (see Appendix). The samples additionally were stained blue to optimize porosity identification. The observations were undertaken in transmitted light, under a standard polarizing microscope. Cement generations were also recognized by means of the cathodoluminescence method (cold cathode), with the voltage of 15 kV and current intensity of 350 mA. A Cambridge Image Technology CLmk3A apparatus, combined with the Nikon Eclipse 50T microscope were used. Porosity types were distinguished with reference to Choquette and Pray's (1970) nomenclature. Two exceptions were made: (1) the term "cavernous porosity" was used for large moulds after the dissolution of brachiopod and/or bivalve shells – typically several centimetres wide, occasionally approaching 1 dm in width; (2) the "channel porosity" referred to interconnected moulds showing some directionality and therefore was treated as a fabric-selective feature.

The zones of intensive dolomitization were recognized on the basis of both standard HCl and Alizarine Red S tests (see Figs 2, 3). The staining procedure started with dissolving 0.1 g of Alizarin Red S in 100 ml of 1.5% HCl (Evamy, 1963). The duration of the reaction was approximately 1 min.

Laboratory measurements (archival data)

The laboratory dataset consisted of approximately 100 archival measurements of helium porosimetry and nitrogen permeability performed on plug samples, the diameter of which was equal to approximately 2.5 cm (Polish Oil and Gas Company). The data were used to: (1) calibrate the log porosity (see below) and (2) analyse the relations between porosity and permeability in the biofacies studied. Porosity-permeability cross-plots were prepared. Average porosity and permeability values were calculated for each biofacies. The correlation between the two parameters was investigated by introducing an exponential fit, as a basis for derivation of the determination coefficients (R^2).

Nuclear magnetic resonance and X-ray microtomography – comparisons

Neither μCT, nor NMR was directly employed in this paper. However, this article provides a short, comparative discussion of the petrophysics of the Brońsko Reef and the adjacent reefs. The Wolsztyn Ridge reef rocks were studied by Fheed and Krzyżak (2017) and Fheed *et al*. (2018), who employed μCT and both low- and high-field NMR experiments, including imaging and relaxometry. The reader is referred to these sources for more details of the procedures applied.

Well log data processing and evaluation

The geophysical analyses comprised the interpretation of and arithmetic operations performed on well log data. *Techlog* software (Schlumberger, 2014) was utilized, including its *Quanti* module, for petrophysical calculations. Caliper (CALI), sonic (DT), gamma (GR), resistivity (shallow – LLS, deep – LLD, microresistivity – MSFL), density (RHOB), neutron (NPHI), and photoelectric (PE) logs were evaluated. The DT, RHOB and LLS logs were used to estimate both total and effective porosity, the GR log was utilized to calculate the shale volume (Vsh), and the set of electric curves, together with the NPHI and PE logs helped to demonstrate the potential presence of fractures and/or natural gas (see below).

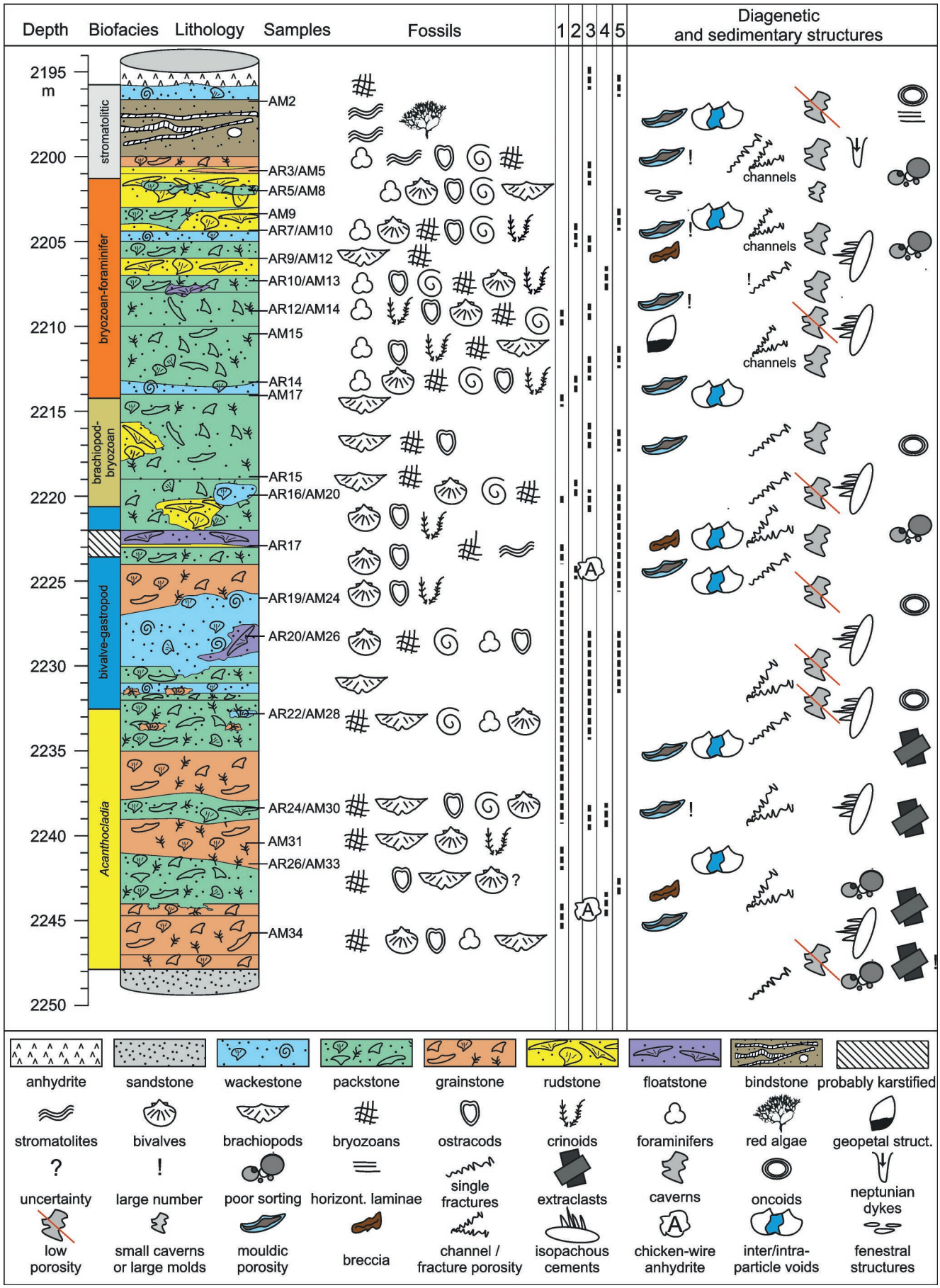

Fig. 2. Brońsko-1 well: biofacies and lithological profile. The dashed, numbered lines next to the profile correspond to: 1 – dolomites, 2 – dolomitic limestones, 3 – anhydrite cementation, 4 – quartz occurrences, 5 – stylolitization (chemical compaction).

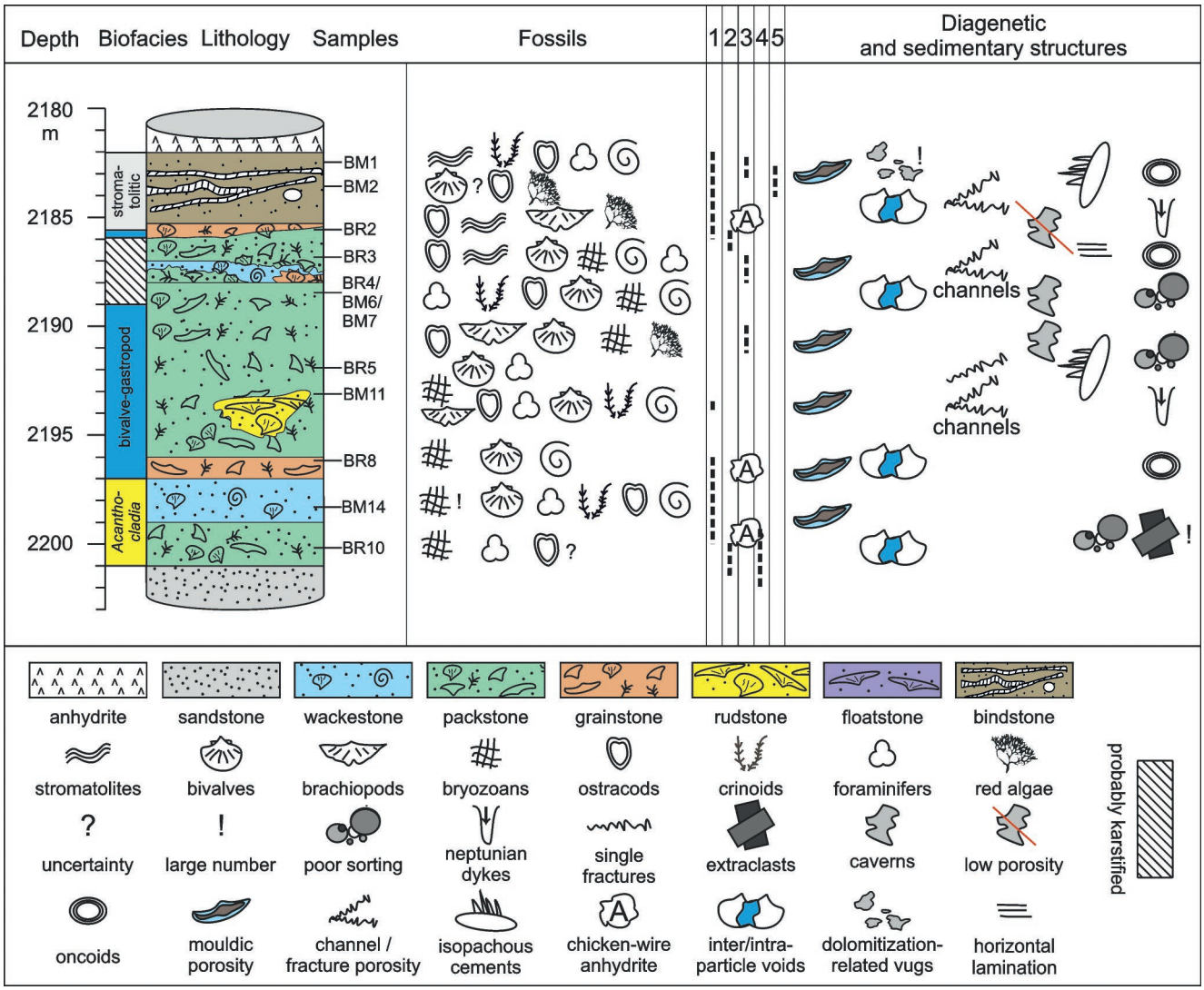

Fig. 3. Brońsko-2 well: biofacies and lithological profile. The dashed, numbered lines next to the profile correspond to: 1 – dolomites, 2 – dolomitic limestones, 3 – anhydrite cementation, 4 – quartz occurrences, 5 – stylolitization (chemical compaction).

Quantitative data derivation procedures

For the needs of porosity derivation, a table of tentative lithofacies was prepared to subdivide the data into groups of similar lithology (see Table 1). Thus, specific parameters could be assigned to a given zone (Table 1).

The PHIT (S) porosity (total sonic porosity) was calculated using the equation of Wyllie *et al*. (1958; Eq. 1):

$$PHIT\ (S) = \frac{DT - DT_{ma}}{DT_{fl} - DT_{ma}} \qquad \text{(Eq. 1)}$$

Where:

PHIT (S) = Total porosity calculated from the sonic log [v/v]

DT = Sonic log reading [μs/ft]

DT_{ma} = Matrix transit time [μs/ft]

DT_{fl} = Fluid transit time [μs/ft] – here 189 [μs/ft]

Here, the DT_{fl} value had to be assumed, as this drilling information was lacking. According to Schlumberger (1989), its value is usually close to 189 μs/ft. The DT_{ma} value, in turn, was assigned carefully in three steps. Firstly, the general lithological and mineralogical composition of the interval of interest was resolved from core description and polarized microscopy data. Secondly, a characteristic DT_{ma} value was specified for each mineral. The last step was to calculate the average DT_{ma} value. The weighted average method was used and the weights depended on the previously estimated amount of each mineral phase. The resulting DT_{ma} values were substituted into Eqation 1 to give the PHIT (S) values.

For comparison purposes, the total porosity was also calculated from the RHOB log. The procedure was analogous to the one above, but here the matrix density parameter (ρ_{ma}) was estimated. The total porosity from the density log – PHIT (D) – was derived using Eqation 2 (see Schlumberger, 1989):

$$PHIT\ (D) = \frac{\rho_{ma} - \rho_b}{\rho_{ma} - \rho_f} \quad \text{(Eq. 2)}$$

Where:

PHIT (D) = RHOB log-derived total porosity [v/v]
ρ_{ma} = Matrix density [g/cm^3]
ρ_b = The RHOB log reading [g/cm^3]
ρ_f = Estimated density of the formation fluids [g/cm^3] – here 1

Lastly, the effective porosity was calculated from the shallow resistivity data, as it better corresponds to the effective porosity derived through helium porosimetry. Gas (helium) flow through the sample is determined in the latter, while the strength of opposition to an electric current (resistivity) is examined for the former (see Anovitz and Cole, 2015; Roshnan *et al*., 2019). The modified, Archie's (1942) formula for effective porosity from shallow resistivity was utilized (see Asquith and Krygowski, 2004; Eq. 3):

$$PHIE\ (LLS) = \left(\frac{a}{\frac{R_{xo}}{R_{mf}} S_{xo}^n}\right)^{1/m} \quad \text{(Eq. 3)}$$

Where:

PHIE (LLS) = Effective porosity from the shallow resistivity log [v/v]
R_{xo} = Flushed zone resistivity [Ω·m]
R_{mf} = Mud filtrate resistivity [Ω·m]
S_{xo} = Flushed zone water saturation [Ω·m]
a = Lithology coefficient [-]
m = Cementation exponent [-]
n = Saturation exponent [-]

The *a*, *m* and *n* parameters typically are assigned empirically, and this may be challenging in the case of highly altered carbonate rocks (Ballay, 2012). Therefore, the value of *m* was derived from the calibration of core data. First, an arbitrarily assigned *m* value of 2 (for carbonates, see Ballay, 2012) was substituted into Eqation 3. Then, the *m* values for each lithofacies (Table 1) were modified to fit the helium porosimetry data as closely as possible (see Figs 4, 5). The parameter *a* was treated as a constant (here 1), while *n* was assumed to equal *m* on the basis of Crain's (1986) guidelines for complex rocks. The remaining parameters were provided by the drilling company.

Lastly, the V_{sh} (shale volume) was calculated from the GR log. Here a simple linear model was used (see Asquith and Krygowski, 2004; Eq. 4). The GR_{sh} (shale) value was set as equal to 75 [API], while GR_{ma} (matrix) ranged between ca. 4 and 9 [API]. These values were adjusted manually with reference to the left- and right-hand-side boundaries of the GR response.

$$V_{sh} = \frac{GR - GR_{ma}}{GR_{sh} - GR_{ma}} \quad \text{(Eq. 4)}$$

Where:

V_{sh} = Shale volume [v/v]
GR = The original GR reading [API]
GR_{ma} = The estimated GR reading for rock's matrix [API]
GR_{sh} = The estimated GR reading for 100% shale [API]

Qualitative data interpretation guidelines – fractures and natural gas

Fractures were tentatively recognized from the electric logs. Two signatures were considered: (1) the spikiness of the electric curves, and (2) the crossings of shallow (LLS) and deep (LLD) resistivity logs (see Laongsakul and Dürrast, 2011). In places where the shallow and deep resistivity curves cross, a considerable difference between drilling mud and formation resistivity is taken to indicate the presence of open fractures. In contrast, healed or cemented fractures were identified from very high resistivity values on both curves (cf. Luthi, 2013).

Since the LLS and LLD logs indicate larger dislocations (detected up to tens of centimetres deep into the reservoir), the microresistivity tool giving the MSFL log was found to be the more appropriate for observation of relatively small-scale features, such as dissolution channels (Laongsakul and Dürrast, 2011). These are believed to form numerous spikes on the MSFL curve that registers lower resistivity values, where the channels are open.

Fig. 4. Brońsko-1: well-log interpretation. Preliminary zonation denotes tentative lithofacies recognition for further calculations: B – bindstone, G – grainstone, P – packstone, R – rudstone, D prefix – dolomite, D(-) – slightly dolomitized. Biofacies are indicated to the right of tentative lithofacies. Abbreviations used: F – fractures; Ø – increased porosity; black arrow – increased shaliness (clay minerals). Zones 1 and 2 indicate fracturing. Well-log descriptions: CALI – caliper; PHIT (S)/PHIT (D) – total porosity calculated from sonic (DT) and density (RHOB) logs, respectively; GR – gamma ray; V shale – GR-based shale volume; MSFL, LLS, LLD – electric logs – MSFL: microresistivity, LLS: shallow resistivity, LLD: deep resistivity (note LLS and LLD cross at fractures – zones 1 and 2); PHIE (LLS) – shallow-resistivity effective porosity; He – helium porosity (laboratory data); NPHI – neutron porosity (here decreased owing to the presence of natural gas); PE – photoelectric reading. The names of biofacies are abbreviated (S – stromatolitic, BF – bryozoan-foraminifer, BB – brachiopod-bryozoan, BG – bivalve-gastropod, A – *Acanthocladia*). Stratigraphy: P (Ca1) – Permian (Zechstein Limestone), C – Carboniferous. Reference is measured depth (MD), given in metres.

Table 1

The parameters for porosity calculation with respect to the general lithofacies (see Figs 4, 5).
The order of the lithofacies is given from the bottom to the top, and the DT_{ma} and ρ_{ma} are the calculated matrix transit time and matrix density, respectively – see Equations 1 and 2. The *m* symbol is the cementation exponent utilized in Equation 3

General lithofacies	Abbreviation	Order	Depth Range [m]	DT_{ma} [µs/ft]	ρ_{ma} [g/cm^3]	m [-]
Brońsko-1						
Dolograinstone	DG	1	2233.45 – 2249.05	43.00	2.78	1.75
Dolopackstone/grainstone	DP/G	2	2226.45 – 2233.45	44.00	2.90	1.45
Dolopackstone/rudstone	DP/R	3	2220.55 – 2226.45	45.00	2.86	1.60
Packstone/rudstone with minor dolomitization	P/R D-	4	2209 – 2220.55	46.20	2.82	1.42
Packstone/rudstone	P/R	5	2199.5 – 2209	47.30	2.73	1.82
Bindstone	B	6	2196.25 – 2199.5	47.60	2.78	1.37
Brońsko-2						
Grainstone	G	1	2198.5 – 2201.5	46.60	2.80	1.45
Dolograinstone/dolowackestone	DG/DW	2	2195.5 – 2198.5	45.70	2.78	1.70
Packstone/grainstone	P/G	3	2187.55 – 2195.5	46.96	2.76	1.75
Anh.-rich packstone/grainstone	PGA	4	2185.2 – 2187.55	47,20	2.85	1.19
Bindstone	B	5	2182 – 2185.2	46.40	2.79	2.05

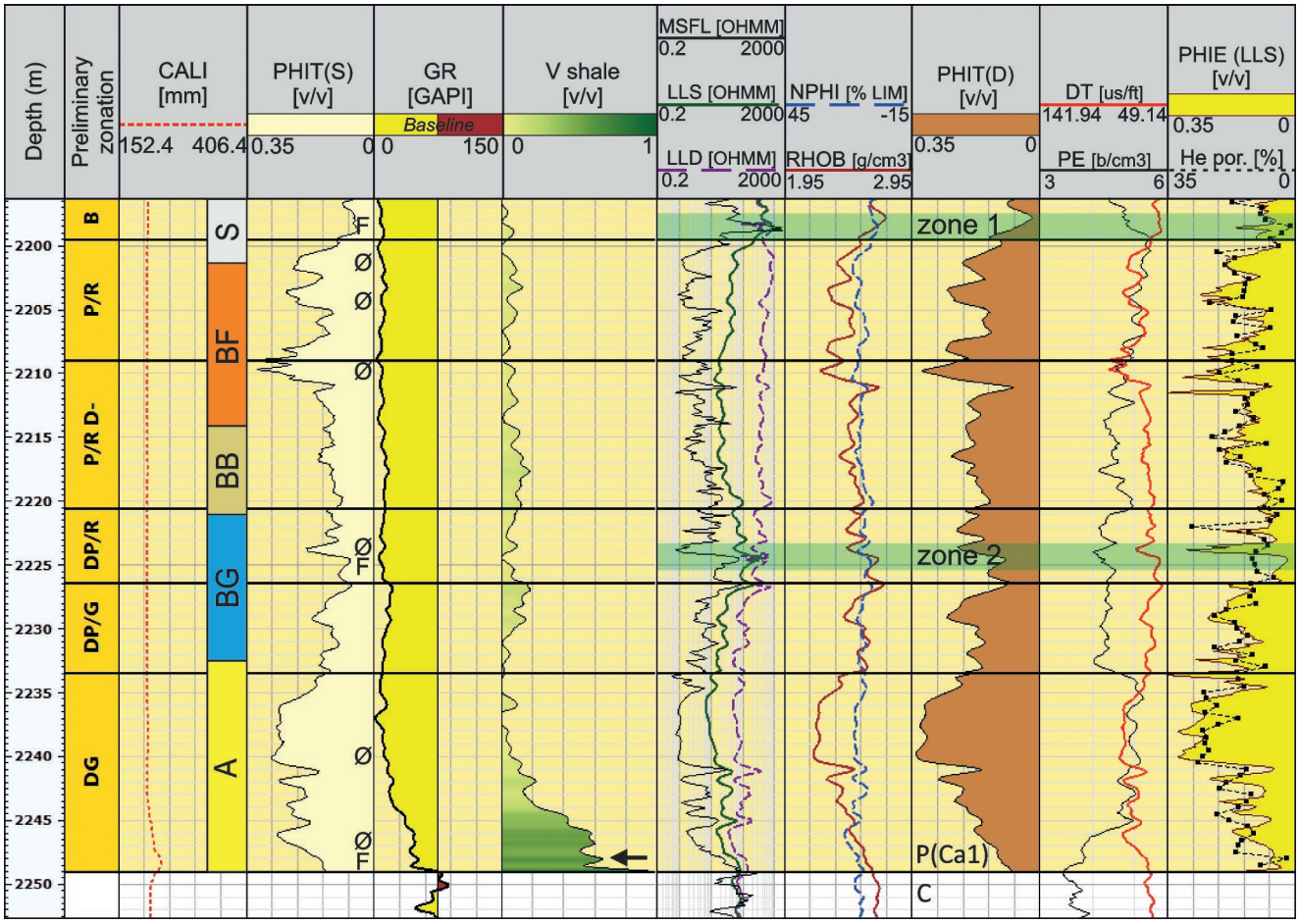

Fig. 4.

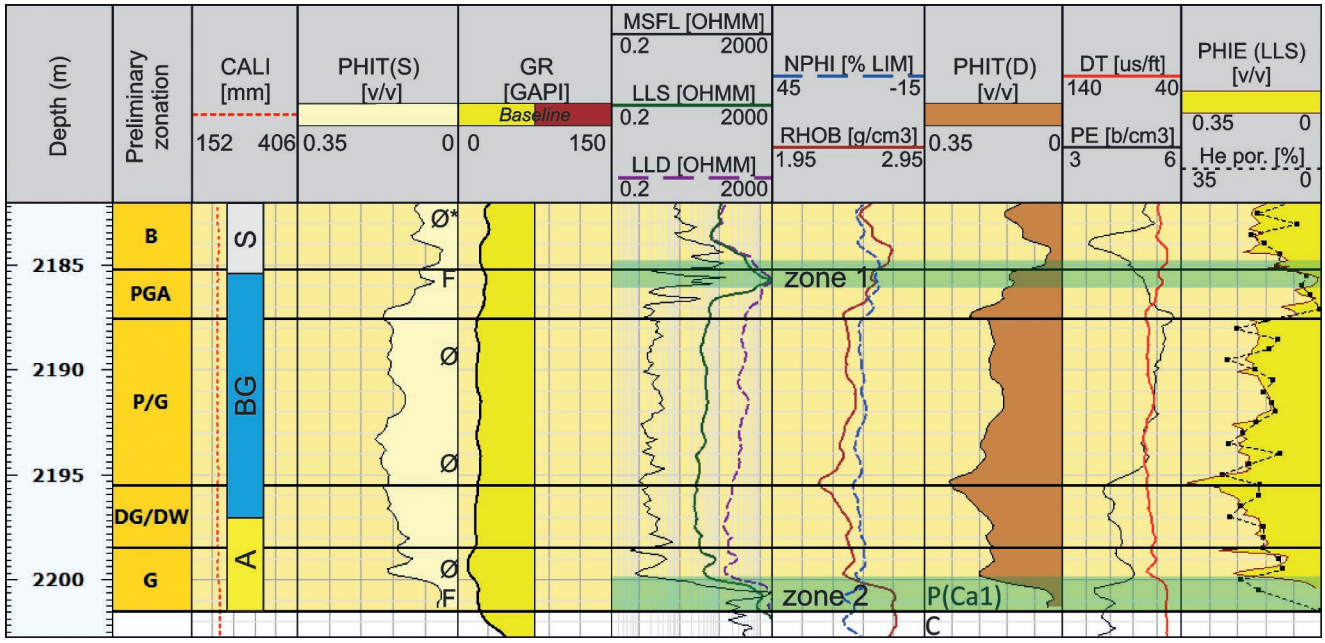

Fig. 5. Brońsko-2: well log interpretation. Preliminary zonation denotes tentative lithofacies recognition for further calculations: B – bindstone, G – grainstone, P – packstone, D prefix – dolomite, PGA – packstone/grainstone with anhydrite. Biofacies are indicated to the right of tentative lithofacies. Abbreviations used: F – fractures; Ø – increased porosity (* – due to the presence of small dolomitization-related vugs). Well log descriptions: CALI – caliper; PHIT (S)/PHIT (D) – total porosity calculated from sonic (DT) and RHOB (density) logs, respectively; GR – gamma ray; MSFL, LLS, LLD – electric logs – MSFL: microresistivity, LLS: shallow resistivity, LLD: deep resistivity (high LLS and LLD resistivity in zones 1 and 2 indicates cemented fractures); PHIE (LLS) – shallow-resistivity effective porosity; He – helium porosity (laboratory data); NPHI – neutron porosity (here decreased owing to the presence of natural gas); PE – photoelectric reading. The names of biofacies are abbreviated (S – stromatolitic, BG – bivalve-gastropod, A – *Acanthocladia*). Stratigraphy: P (Ca1) – Permian (Zechstein Limestone), C – Carboniferous. Reference is measured depth (MD), given in m.

The PE and DT readings indicated the presence of natural gas, where the logs approached each other (cf. Schön, 2015). The presence of natural gas was also confirmed at points of separation of the RHOB and NPHI logs (Schön, 2015).

RESULTS

Basic geological information: Ca1 thickness, fossils and lithology

The Brońsko-2 well shows a much lower thickness of Ca1 strata (19 m), compared to the neighbouring Brońsko-1 well (50 m; cf. Figs 2, 3). Both well sections comprise bioclastic limestones and dolomites, ranging from stromatolitic bindstones – through wackestones, packstones, grainstones and floatstones – to rudstones. A high variability of fossils also was observed. The Brońsko-1 well is dominated by the presence of various types of bryozoans (often encrusted by foraminifers), ostracods, bivalves, gastropods, brachiopods and less common crinoids. The Brońsko-2 well, in turn, excluding its outermost biofacies discussed below, is dominated by molluscs – both bivalves and gastropods – accompanied by bryozoans, ostracods, and other fossils (cf. Figs 2, 3).

Biofacies

Five biofacies were distinguished on the basis of sedimentological and palaeontological analyses (Figs 2–5 for core description and well log information; Fig. 6 for petrophysical properties; Fig. 7 for cement stratigraphy and Figs 8–9 and Figs 10–12 for micro- and macro-scale photographs, respectively). The complete sequence of biofacies was observed in the Brońsko-1 profile and comprises (from the bottom): (1) the *Acanthocladia* biofacies; (2) the bivalve-gastropod biofacies; (3) the brachiopod-bryozoan biofacies; (4) the bryozoan-foraminifer biofacies, and (5) the stromatolitic biofacies. Two biofacies are absent from the Brońsko-2 profile: the brachiopod-bryozoan and bryozoan-foraminifer divisions (cf. Figs 2, 3).

In the two cases studied, the profile starts at the bottom with bioclastic extrasparites (Fig. 11B), containing frequent, albeit strongly fragmented, branched *Acanthocladia* bryozoans (Figs 8A, B, 10A), bivalves (Fig. 10A), and – in the case of the Brońsko-1 well – also single terebratulid brachiopods, more common in the overlying biofacies. The bryozoans are often encrusted, either by foraminifers or ostracods (see Figs 8G, 9G, 10G, cf. Fig. 8B, showing moulds of mixed origin). Encrusting bryozoans also frequently surround the bivalves (Fig. 10A). Some of the bivalve shells close to the bottom of the *Acanthocladia* biofacies exhibit a prismatic structure (Fig. 9B).

The rocks mentioned above are covered by the bivalve-gastropod biofacies, with numerous, undamaged bivalve shells – typically *Bakevellia* or *Liebea* (Figs 8D, 10B, 11D) – gastropods (Figs 8D, 9C, 11A) and less common ostracods, brachiopods, bryozoans and foraminifers, including

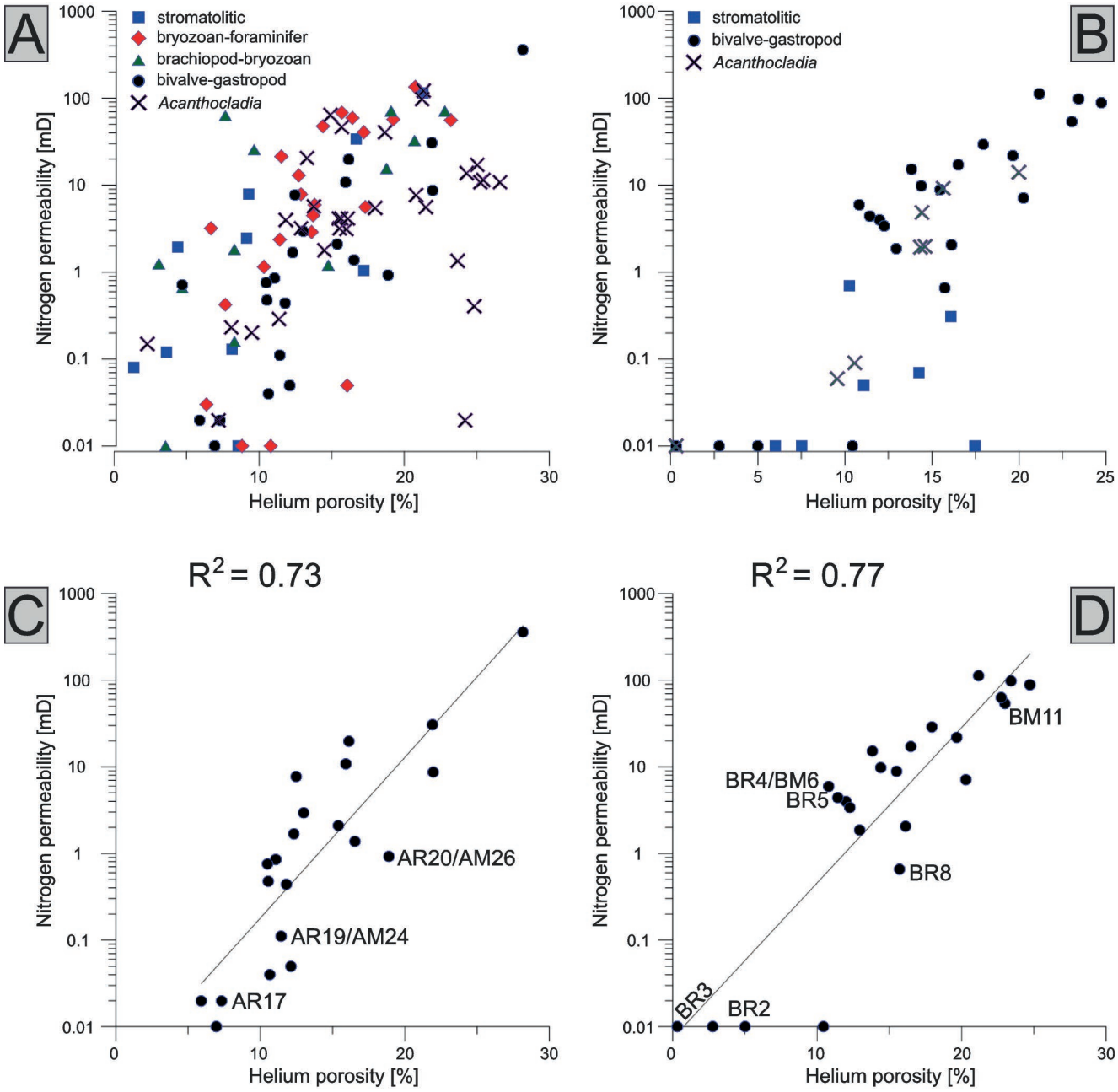

Fig. 6. Porosity-permeability cross-plots. **A, B.** Whole-core datasets for strata of Brońsko-1 (A) and Brońsko-2 (B). The measurement points were assigned to particular biofacies and marked with distinctive symbols presented in the figure. The points in **C** (Brońsko-1) and **D** (Brońsko-2) were limited to the bivalve-gastropod biofacies, where an exceptionally high porosity-permeability correlation was observed. R^2 is the determination coefficient.

encrusting and uniserial genera (Figs 8C, D, 12D). This biofacies covers almost three-quarters of the Brońsko-2 profile (Figs 3, 5), where it is directly followed in vertical sequence by the stromatolitic or microbial biofacies (Figs 8I, 10H). The bivalve-gastropod biofacies of the Brońsko-2 well is often accompanied by even more foraminifers (Figs 3, 8C, D). In both wells, scarce crinoids occur (Figs 2, 3). The biofacies is also anhydrite-rich (see the "Cement stratigraphy" section below).

Next, the brachiopod-bryozoan biofacies was developed at the Brońsko-1 location. The biofacies is missing in the Brońsko-2 well. It contains numerous, small and well-preserved brachiopod shells: mainly terebratulid (but also strophomenid; Figs 8E, 9E, F). Some of these also can be traced in the bivalve-gastropod biofacies (Fig. 11E). In places, *Dielasma* also occurs (see Fig 11C).

At the Brońsko-1 well location, where there is a much greater thickness of the Ca1 strata, the deposition of the stromatolitic biofacies (Fig. 8H) was preceded by the formation of the bryozoan-foraminifer biofacies. This contains a variety of bryozoan genera – from branched, through columnar, encrusting to fenestrate – mainly *Rectifenestella* and *Kingopora* (cf. Figs 8F, G, 10D–G). In this case, the extremely frequent foraminifers usually encrusted the bry-

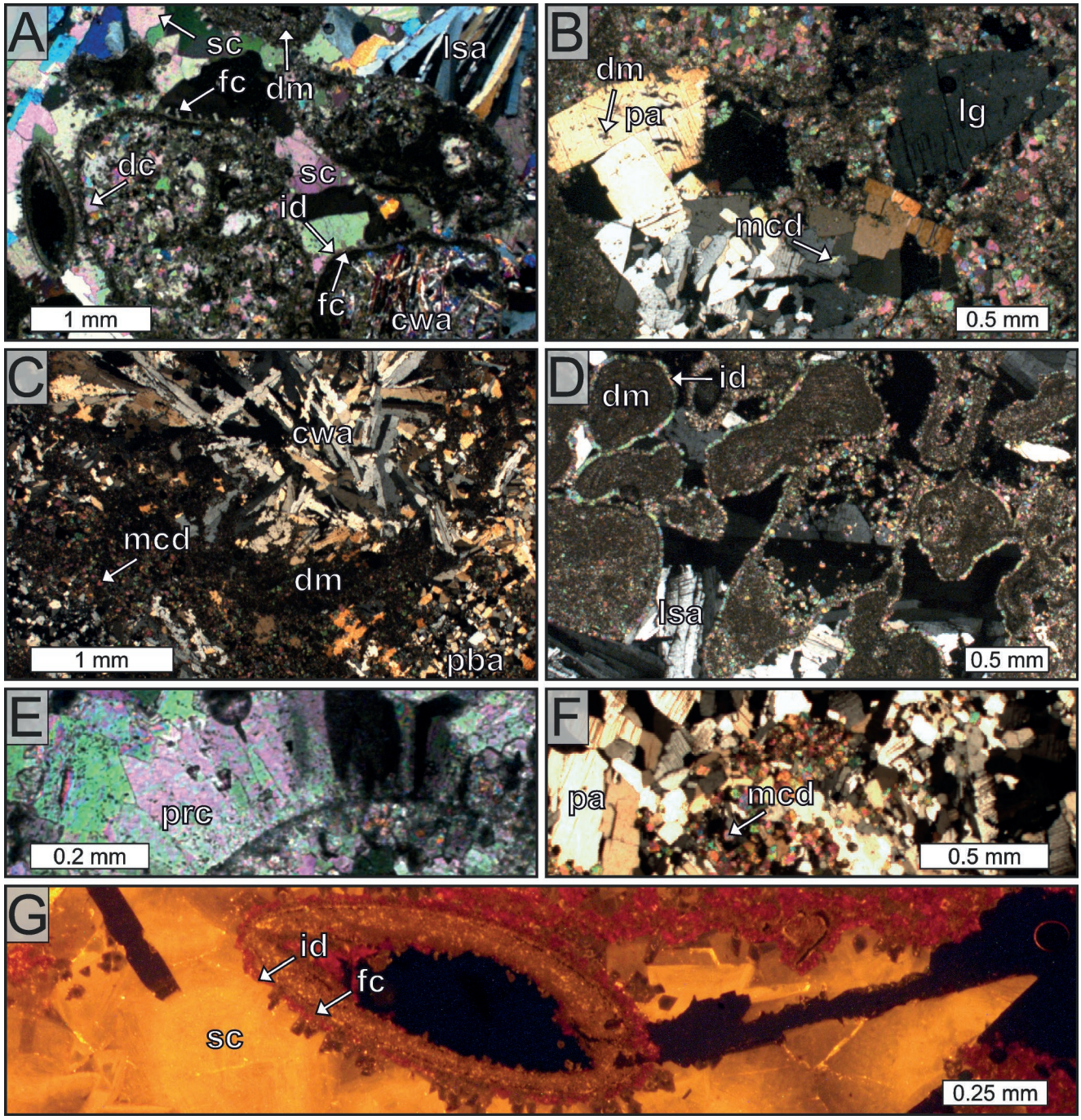

Fig. 7. Microscope observations. **A.** Several generations of cements including dolomicrite, well-preserved fibrous calcite followed by isopachous dolomite (see picture **G**), and both chicken-wire and lath-shaped anhydrite. Sparry and drusy (burial) calcite are also present; BM11. **B.** Sparry, poikilotopic anhydrite cement with dolomitic inclusions and single lenticular gypsum crystals (?); AM10. **C.** Sabkha-related, chicken-wire and pile-of-bricks anhydrite preceded by dolomicrite, in the neighbourhood of medium-crystalline dolosparite; AR19. **D.** Isopachous dolomite cement rimming the bioclasts (mostly gastropods), following the dolomicrite surrounded by younger, lath-shaped anhydrite; AR22. **E.** High magnification of prismatic calcite crystals; AR5. **F.** Medium-crystalline dolosparite in the vicinity of the poikilotopic anhydrite; AR17. **G.** Marine fibrous calcite rimming an ostracod shell, followed by isopachous dolomite and sparry burial calcite; a magnification of A; BM11. Cement abbreviations: dc – drusy calcite, fc – fibrous calcite, prc – prismatic calcite, sc – sparry calcite, dm – dolomicrite, id – isopachous dolomite, mcd – medium-crystalline dolosparite, cwa – chicken-wire anhydrite, lsa – lath-shaped anhydrite, pa – poikilotopic anhydrite, pba – pile-of-bricks anhydrite, lg – lenticular gypsum (?). Cross-polarized light (except for G – cathodoluminescence). Sample annotations are marked with capital letters followed by a number (cf. Figs 2, 3).

ozoans (Figs 9G, 10G). They can be found particularly in the upper part of the biofacies. Numerous gastropods and bivalves continued to develop here (Figs 8G, 9H) among frequent ostracods (Fig. 8F) that also surrounded the bryozoans. In some places, single brachiopods also occur. Relatively scarce crinoids and even sea urchins were found in this biofacies.

Ultimately, as in the case of the Brońsko-2 well, the Ca1 strata of Brońsko-1 terminates upward with the stromatolitic biofacies (Fig. 8H), showing a relative scarcity of fossils, including, for example single bryozoans, rare red algae, ostracods and gastropods.

Cement stratigraphy and remaining diagenetic processes

In the case of the Brońsko-1 sequence, the rocks of the brachiopod-bryozoan, bryozoan-foraminifer and stromatolitic biofacies frequently are cemented with micritic calcite (Fig. 8F and H). In the remaining biofacies, including most of the strata in the Brońsko-2 well, dolomicrite is present instead (Figs 7A, C, D, 9D) and within the stromatolitic biofacies, it is cut by calcite veins and contains numerous vugs (Figs 8I, 11H). The micritic cements are followed by different forms of calcite, from equant, through bladed to fibrous (Fig. 7A, G). Such cements were observed mainly in the upper part of Ca1 profile, that is, in the bivalve-gastropod biofacies (Brońsko-2) and the bryozoan-foraminifer biofacies (Brońsko-1). Some of the calcite cements were recrystallized as prismatic forms (Figs 7E, 9B). The calcite cements are often surrounded by isopachous, planar, medium- to fine-crystalline dolosparite, forming isopachous rims around the bioclasts. They are particularly common in the *Acanthocladia* and bivalve-gastropod biofacies (Fig. 7A, D, G).

The cements mentioned above frequently are cut by fractures (e.g., Fig. 12B). In places, the fractures are accompanied by partially brecciated rocks (Fig. 12C) and neptunian dykes, occurring particularly close to the tops of the bivalve-gastropod and bryozoan-foraminifer biofacies. Numerous, large vugs and caverns are characteristic among the features mentioned (Fig. 12B). Close to the top of the bivalve-gastropod biofacies, the number of fractures abruptly increases. At that location, the fractures form well-organized, subvertical and horizontal systems that resemble pseudokarren and in places are filled with barite and less common ferroan oxides, red in colour and of questionable origin (see the discussion and Fig. 12B).

The next generation of cement is medium-crystalline dolosparite (Figs 7B, C, F, 8C, 9D), forming inclusions within the succeeding poikilotopic anhydrite (Fig. 7B, F). Single, sharp-ended, lenticular gypsum bodies also may be observed in the upper part of the Ca1 profile (Fig. 7B). The medium-crystalline dolosparite is the most common for the lower portion of Ca1 and frequently can be found in the bivalve-gastropod and Acanthocladia biofacies. Among the sulphates, anhydrite is much more common than gypsum and appears in at least four main forms: (1) as chicken-wire crystals (Figs 7A, C, 8C), (2) in a pile-of-bricks fabric (Fig. 7C), (3) as lath or rosette shapes (Figs 7A, D; 8B, D, 9D), and (4) as poikilotopic, sparry cement (Fig. 7B, F). Anhydrite is most abundant in the bivalve-gastropod and brachiopod-bryozoan biofacies, where chicken-wire crystals and pile-of-bricks fabrics are very common. The latter show signs of physical compaction (see the "Reconstruction of diagenetic history" section). A sparry, lath-shaped anhydrite is more common for the bryozoan-foraminifer biofacies. The sulphates tend to be followed by another generation of medium-crystalline dolosparite, precipitated along anhydrite cleavage surfaces. This generation of dolomite typically occurred before the sparry (Figs 7A, G; 8H, 9C), drusy (Fig. 7A, 8G) and the prismatic calcite crystals (Figs 7E, 9B), particularly common within the bryozoan-foraminifer biofacies. Horizontal stylolites are locally present and frequently cut the cements mentioned above (see Figs 2, 3). They can be accompanied by late fractures (see Fig. 8A).

Porosity – general remarks

Five major porosity types were observed: (1) mouldic porosity, the most common (e.g., Figs 8B, C, 9F, H, 10A, 11C); (2) well-developed fractures and dissolution channels (e.g., Figs 8A, E, H, 9G, 11D, 12B); (3) vuggy and cavernous voids (e.g., Figs 8G, 10B, C, 11E, F, 12A, B); (4) intra- and interparticle porosity (e.g., Figs 8B, F, 9A, C, E, 10F, 11G, 12D); and (5) dolomitization-related intercrystalline voids (e.g., Fig. 8B). All the porosity types distinguished were encountered in the Brońsko-1 well, which is more palaeontologically and petrophysically diversified than its Brońsko-2 neighbour (e.g., Fig. 8G). The rocks coming from Brońsko-2 well exhibit a noticeable predominance of mouldic porosity (Fig. 10A), which is less common for the Brońsko-1 strata. The moulds are often connected with ostracods (Fig. 8F), bivalves (Fig. 10A), gastropods (Fig. 11A), and small *Dielasma* brachiopod coquinas (Fig. 11C). In addition to the vugs mentioned in the previous chapters, intraparticle pores after dolomitized microbial structures can also be found (Fig. 11G).

Similar trends of porosity decrease are repeated in both wells. Three zones of decreased porosity (cf. Figs 4, 5) can be seen: (1) the sulphate-cemented intervals of the bivalve-gastropod and brachiopod-bryozoan biofacies (Fig. 10B); (2) the vug-free stromatolite biofacies (Brońsko-1, Fig. 8H); and (3) the extraclast-rich, lowermost interval of the *Acanthocladia* biofacies (Fig. 11B). In the places listed, the total porosity can even fall below 5%, as indicated by well log and laboratory data (see Figs 4–6 and Appendix).

Considerable porosity increases were noted for the bryozoan-foraminifer biofacies, represented by numerous caverns, moulds, channels (Fig. 8F) and intraparticle voids related to dissolved bryozoan zoecia (see Fig. 8F, G). Similarly, the unfilled caverns and moulds, occurring in both the brachiopod-bryozoan and bivalve-gastropod biofacies, account for local porosity increases. The coherently developed moulds present in the *Acanthocladia* biofacies (Figs 8B, 10A, 11A) also seem to significantly improve the porosity.

The channels frequently are accompanied by fractures, detectable at different levels of observation, including macro-scale core analyses (Figs 2, 3, 12B), microscope studies (Fig. 8A, E) and resistivity logs (LLS and LLD crossings; see Fig. 4, zones 1 and 2). Both anhydrite and calcite have

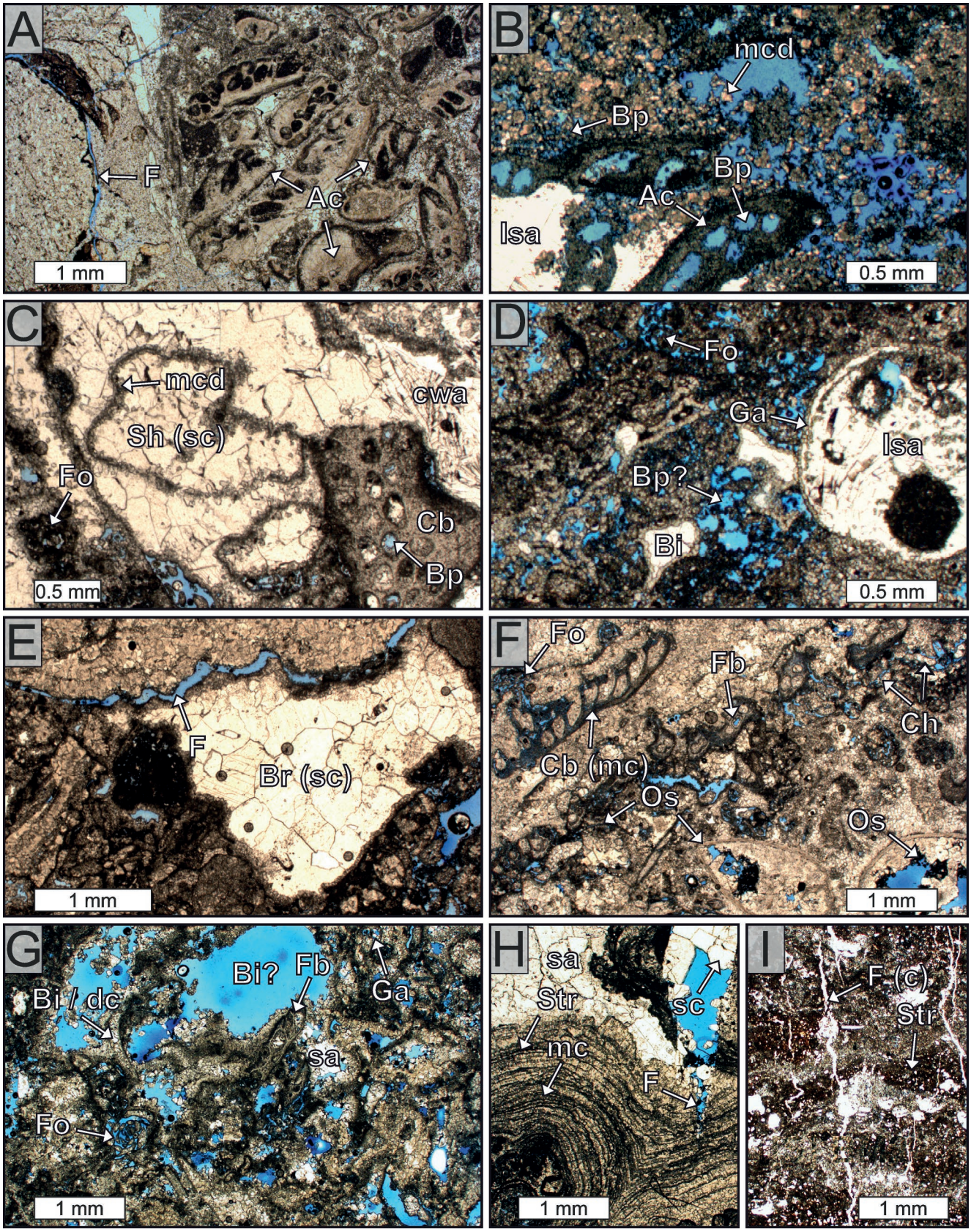

Fig. 8. Microscope observations. **A.** Well-preserved *Acanthocladia* bryozoans (zoecia filled with sediment), surrounded by scarce fractures; AR26. **B.** Crushed *Acanthocladia* bryozoan fragments (zoecia dissolved – intraparticle porosity), often encrusted by foraminifers prior to dissolution – note numerous moulds related to both bryozoans and foraminifers, and dolomitization-related intercrystalline porosity; BR10. **C.** Bivalve-gastropod biofacies showing numerous shells with dolomitized outlines, cemented with sparry burial calcite, in places accompanied by chicken-wire anhydrite. The shells are often encrusted by foraminifers and scarce ostracods, and surrounded by columnar bryozoans with well-preserved intraparticle porosity; BM11. **D.** Bivalve-gastropod biofacies containing gastropod shells

filled a considerable volume of fractures, especially in the upper part of the reef (see Figs 2, 3, 5, high resistivity in zones 1 and 2, 8I).

Detailed relations between porosity/permeability and biofacies

The *Acanthocladia* biofacies

The *Acanthocladia* biofacies appeared to have strong potential for the formation of mouldic and intraparticle porosity (Figs 8B, 10A, 11A). The mouldic pores account for a total porosity of around 30%, locally approaching or falling below 10% towards the Carboniferous, as indicated by the PHIT (S) and PHIT (D) curves (see Appendix; Figs 4–6). In the case of the Brońsko-1 well, an average effective porosity from shallow resistivity – PHIE (LLS) – oscillates around 18% (with a minimum of 5%), compared to roughly 17% from helium porosimetry (Appendix; Figs 4, 6A). For the Brońsko-2 well, the corresponding values are ca. 12.5% and 13%, respectively (Appendix; Figs 5, 6B).

Despite considerable fragmentation of the branched bryozoans, in places their larger fragments with well-preserved zoecia were the focus of intensive dissolution and thus intraparticle porosity, often linked to columnar and encrusting bryozoans, was formed (see Figs 8B, 9A, 12D). This kind of porosity, along with small vugs also is enhanced by single, dissolved shells of bivalves and gastropods, occurring close to the base of Ca1 (Fig. 10A). Moreover, even if fragmented, the bryozoans tended to be encrusted by numerous foraminifers, or less commonly by ostracods. It also was observed that in the presence of single foraminifer encrustations, the permeability exceeds 100 mD, which is a relatively high value for the Brońsko Reef (see Appendix; Fig. 6). Such a situation is more common for the strata in Brońsko-1, which contain more channels by comparison with Brońsko-2 (cf. Fig. 6A, B). Despite that, a very weak correlation between porosity and permeability exists. The determination coefficient (R^2) is as low as 0.17 for the rocks from Brońsko-1. The permeability changes from ca. 0–120 mD, and is generally higher for Brońsko-1 (averagely 16.5 mD, as compared with 4.02 mD for Brońsko-2; see Appendix; Fig. 6A, B). It should be added that the potential dissolution channels are much less common here than for the bryozoan-foraminifer biofacies, where the number of such structures is striking. The channels often co-occur with fractures and they both can be traced on the spiky MSFL log (see Fig. 4). Flat fragments of the log indicate the predominance of moulds over fractures, which is typical for this biofacies. More moulds appear in the case of the Brońsko-2 section (Fig. 3), but here the resistivity readings suggest the presence of cemented fractures (see Fig. 5).

Drusy calcite is present between the bioclasts (cf. Fig. 7A). The cements reduced a significant portion of voids especially in the case of Brońsko-2 (see the PHIT (S) plot in Fig. 5). The porosity also was reduced by isopachous dolomite cement and sparry calcite veins, the role of which was discussed below in the "Reconstruction of diagenetic history" section.

The biofacies is dolomitized and/or cemented with dolomite (see Figs 2, 3, 8B). In Brońsko-1, however, more limy horizons occur among the dolomitized strata (cf. Figs 2, 3). Dolomitization is particularly common in places where the RHOB log shows local maxima (Figs 4, 5). Some of the readings are hardly interpretable owing to an elevated gas content in this interval (see the NPHI and RHOB curves showing increased separation, as well as the PE and DT curves approaching each other in Figs 4, 5). However, the dolomitization is much less pronounced here in comparison to the bivalve-gastropod biofacies, described below (cf. Fig. 9D). The density (RHOB) of the *Acanthocladia* biofacies increases abruptly towards the bottom, where more anhydrite and Carboniferous extraclasts occur (see Figs 4, 5, 11B).

Lastly, it is worth mentioning the brecciation of Ca1 rocks observed within the *Acanthocladia* biofacies. The breccia to some degree was fractured. Such structures are particularly common close to the base of Ca1 (cf. Fig. 8A). However, the majority of fractures are filled with clay and other accompanying minerals.

The bivalve-gastropod biofacies

Bivalves, depending on their size, contributed to the evolution of mouldic and/or cavernous porosity (Fig. 10B). Large intraparticle voids were created specifically within the gastropod shells (Fig. 9C), accompanied by small terebratulid brachiopod (*Dielasma*) coquinas (Fig. 11C),

---

(filled with lath-shaped anhydrite), bivalves, crushed and dissolved *Acantholcadia* bryozoans leaving moulds, and dissolved encrusting foraminifers (forming channel porosity); BR8. **E.** Brachiopod-bryozoan biofacies – both fragmented and complete brachiopod shells (often cemented with sparry burial calcite), in the vicinity of small moulds, vugs and fractures; AR15. **F.** Fossil-rich bryozoan-foraminifer biofacies with intraparticle, mouldic, channel and vuggy porosity. Observe the presence of moulds and intraparticle voids after the dissolution of ostracod shells. Also note the fragmented fenestrate and columnar bryozoans, slightly improving the intraparticle porosity; AR5. **G.** Bivalve-rich bryozoan-foraminifer biofacies with large cavernous voids. Also note the drusy calcite and sparry anhydrite; AM10. **H, I.** Stromatolitic biofacies with single fractures (in I filled with calcite; note the cemented vugs/fenestral pores). Micritic calcite is common here; (H – AM2, I – BM2). Ac – *Acanthocladia* branched bryozoan fragments, Cb – columnar bryozoans, Fb – fenestrate bryozoans, Bp – bryozoan-related porosity, Bi – bivalves, Br – brachiopods, Ch – channel porosity, F – fractures, Fo – foraminifers, Ga – gastropods, Os – ostracods, Sh – unidentified shells, Str – stromatolites. Cement abbreviations: c – calcite (veins), mc – micritic calcite, dc – drusy calcite, sc – sparry calcite, lsa – lath-shaped anhydrite, sa – sparry anhydrite, mcd – medium-crystalline dolosparite, cwa – chicken-wire anhydrite. Transmitted-light microphotographs, plane-polarized light. Porosity is stained blue. Sample annotations are marked with capital letters followed by a number (see Figs 2, 3).

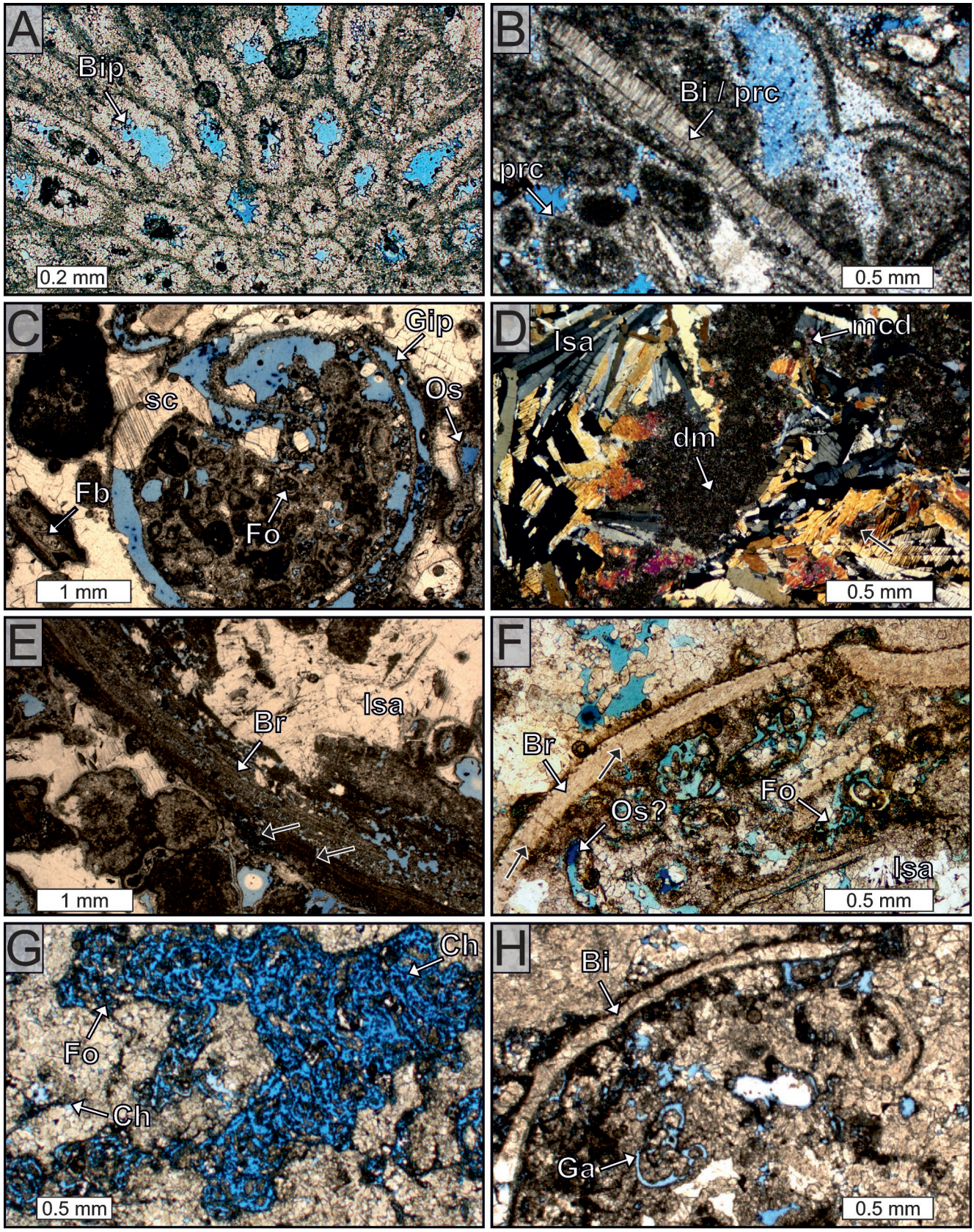

Fig. 9. Microscope observations. **A.** *Acanthocladia* biofacies – well-preserved intraparticle porosity within the zoecia of columnar bryozoans; AR24. **B.** Prismatic structure (calcite) of some bivalve shells occurring within the *Acanthocladia* biofacies. Note isopachous prismatic calcite rims (arrowed), surrounding the bioclasts; AM34. **C.** Bivalve-gastropod biofacies with a large gastropod dissolved to form intraparticle porosity – note fragmented bryozoans and foraminifers inside the shell; BM11. **D.** Heavily cemented, micritic, and poorly porous part of the bivalve-gastropod biofacies – note the lath-shaped anhydrite crystals, fully dolomitized matrix (dolomicrite), the medium-crystalline dolosparite, and dolomicrite inclusions within the anhydrite cement (black arrow); BM11. **E.** Terebratulid brachiopod

improving the potential for preservation of mouldic porosity. However, both moulds and intraparticle voids usually have been cemented widely with chicken-wire, poikilotopic and lath-shaped anhydrite, leaving only single voids open (Figs 2–5, 7C, D, F, 8C, 9D, 10B, 11D). Locally, they also were filled with barite and ferroan oxides (see Fig 12B). More unfilled moulds and channels can be observed in the rocks from the Brońsko-2 well (see Figs 3, 5, 8D). Where anhydrite cementation was intensive, a corresponding porosity decrease could be observed, especially in the Brońsko-2 section, as seen in the PHIT (S), PHIT (D) and PHIE (LLS) curves in Fig. 5 and in the spiky character of the DT log. The total porosity reaches even 25% and 28% for Brońsko-1 and Brońsko-2, respectively, as shown by the PHIT (D) plot (see Figs 4, 5). In both cases, the effective PHIE (LLS) porosity typically reaches 20%, with an average value of around 14%, as compared with 13–16% indicated by helium porosimetry (Figs 4, 5, 6C, D; Appendix). The minimum values of PHIE (LLS) are 3% and 1% for the Brońsko-1 and Brońsko-2 strata, respectively. The former has a maximum permeability of 360 mD (Fig. 6C), while the latter exhibits up to 115 mD (Fig. 6D). However, in the case of Brońsko-2, more non-permeable samples were examined (see Appendix; Fig. 6C, D). The corresponding average values of this parameter are very similar: 21.36 and 23.83 mD, respectively (Appendix). The correlation between porosity and permeability is moderate, with R^2 values of about 0.70, in both cases. Moreover, the cemented fragments of shells frequently have been significantly fractured – especially in the case of Brońsko-1 (cf. Fig. 4 – zone 2, Fig. 11D). This is associated with the karst features described above (Fig. 12A, B). The channels are more common than intercrystalline pores, which are quite rare in the bivalve-gastropod biofacies of the Brońsko-2 well.

The Brońsko-1 (Ca1) rocks were dolomitized much more intensively (cf. Figs 2, 3). Here, the majority of bioclasts appearing in the lower part of the biofacies have been dolomitized (Fig. 2; Appendix), mainly in a texture-destructive pattern. This can be demonstrated for an analogous, exceptionally strongly dolomitized section of the Brońsko-2 well (Fig. 9D). However, the precipitation of sparry calcite (Fig. 8C) significantly reduced the porosity of the biofacies.

The brachiopod-bryozoan biofacies

The brachiopod and bryozoan fragments significantly contributed to the formation of cavernous porosity (Fig. 10C). Many caverns were cemented extensively with both chicken-wire and lath-shaped anhydrite (cf. Figs 2–5, 7C, D, 9F) and sparry calcite. These cements considerably decreased the porosity (cf. Figs 4, 9E). Single moulds remained unfilled, in contrast to large, typically cemented caverns. The total geophysical porosity changes between 10%, indicated by the PHIT (S) curve, and 23% from the PHIT (D) plot (Fig. 4). The effective porosity from the resistivity log – PHIE (LLS) – ranges from 2% to over 20%, with an average of ca. 13%, as opposed to just 11.8% indicated by helium porosimetry (Figs 4, 6A; Appendix). The permeability is low and reaches a maximum of 72 mD, with the minimum value approaching 0 mD (Fig. 6A; Appendix). Poor correlation between porosity and permeability exists (R^2 is 0.46).

Excluding the places of intensive leaching marked by the presence of large, open, brachiopod-related caverns (Fig. 10C), no significant porosity increases were noted (see the PHIT (S) and PHIT (D) curves in Fig. 4).

A positive aspect in terms of porosity gain is the fact that the bryozoan (mainly branched and columnar) fragments were extensively dissolved, leaving mouldic, relatively poorly developed channel porosity and intraparticle porosity (cf. Fig. 8F). On the other hand, this biofacies does not show any significant influence of fracturing; single fractures cut the strata (e.g., Fig. 8E), as confirmed by the relatively smooth resistivity curves (Fig. 4). Nor is it considerably dolomitized (Fig. 2). Only single dolomite crystals can be traced under the polarizing microscope, chiefly in a form of a fine- or medium-crystalline dolosparite occupying the carbonate matrix.

The bryozoan-foraminifer biofacies

This biofacies shows the greatest variability of fossils. It could not be distinguished in the case of the Brońsko-2 well, since bryozoans were less common than bivalves and gastropods (cf. Figs 2, 3). The fenestrate bryozoans occurring among both branched and columnar genera are relatively poorly preserved and fragmented (Figs 9C, 10G). In places, their large, well-preserved fragments accounted for the maintenance or development of some proportion of intraparticle voids (Fig. 10D). The columnar bryozoans also increased this type of porosity (Fig. 10F). In addition to the intraparticle, bryozoan-related pores, the moulds and channels after frequently occurring dissolved skeletons of foraminifers (and ostracods) are also common (Fig. 9G). Here, channels occur much more often than in the *Acanthocladia* biofacies, where the outlines of the foraminifers are

---

with typical shell lamination and natural, crosswise, intraparticle pores (black arrows), occurring in the lowermost part of the bivalve-gastropod biofacies. The brachiopod is surrounded by gastropods, branched bryozoans and foraminifers (forming moulds and channels). Note the lath-shaped anhydrite; AR22. **F.** Terebratulid brachiopod at the transition between the bryozoan-foraminifer and bivalve-gastropod biofacies; note the natural intraparticle pores (black arrows) and numerous foraminifer/ostracod-related moulds; AM15. **G.** Typical dissolution channels after encrusting foraminifers in the bryozoan-foraminifer biofacies – the channels show variable diameters/bandwidths; AR3. **H.** Bryozoan-foraminifer biofacies showing bivalve, gastropod and other fragmented shells. Note the mouldic porosity and small dissolution vugs; AM15. Bip – Bryozoan-related intraparticle porosity, Bi – bivalve shells, Fb – fenestrate bryozoans, Br – brachiopods, Fo – foraminifers, Ch – channel porosity, Ga – gastropods, Gip – gastropod-related intraparticle voids, Os – ostracods; cement abbreviations: prc – prismatic calcite, sc – sparry calcite, dm – dolomicrite, mcd – medium-crystalline dolosparite, lsa – lath-shaped anhydrite. Transmitted-light microphotographs, plane-polarized light except for D (cross-polarized). Porosity is stained blue. Sample annotations are marked with capital letters followed by a number (see Figs 2, 3).

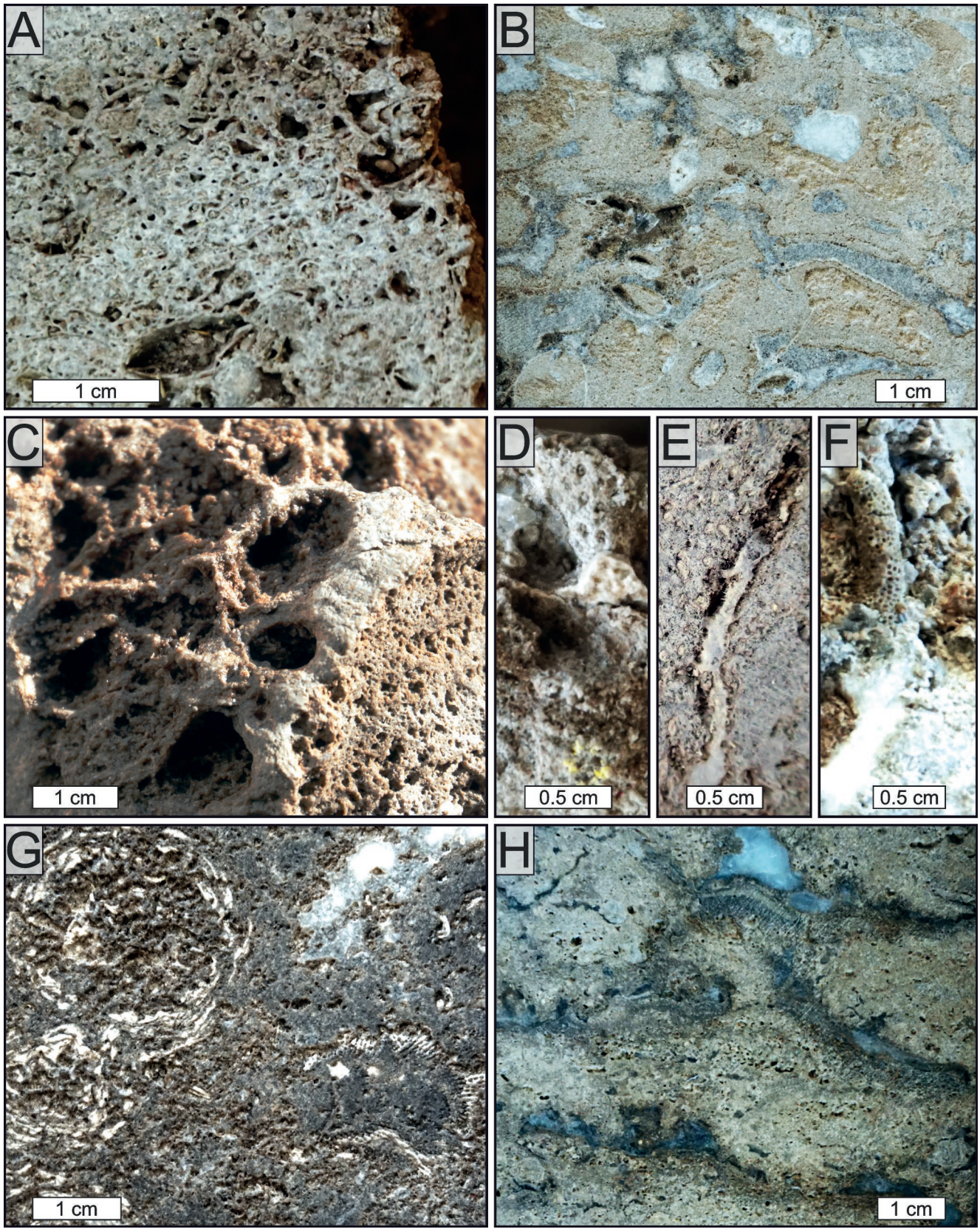

Fig. 10. Drill core photographs. **A.** *Acanthocladia* biofacies – intraparticle/mouldic porosity after fragmented branched bryozoans in the vicinity of moulds and caverns related to bivalve shells (2198, B2) **B.** Bivalve-gastropod biofacies – both anhydrite-cemented and open bivalve caverns surrounded by gastropods (2221, B1). **C.** Brachiopod-bryozoan biofacies enclave – large open caverns after unidentified shells (probably terebratulid brachiopods). Note small moulds and intraparticle pores (probably of microbial origin) in the lower right corner of the photograph (2214, B1). **D–F.** Brachiopod-foraminifer biofacies – different bryozoan genera – D: fenestrate (*Kingopora*), E: branched (*Acanthocladia*), F: columnar (with intraparticle porosity still preserved) (2204–2206, B1). **G.** Bryozoan-foraminifer biofa-

far less recognizable (cf. Fig. 8B). The presence of channels is noticeable in the form of spikes on the MSFL curve presented in Figures 4, 5.

Lastly, it is noteworthy that a significant proportion of the cavernous porosity typically is associated with bivalves and brachiopods (see Figs 8G, 12A). Such caverns often remained open. Multiple spikes can be observed on the acoustic log, owing to their presence. This is seen in the zones of increased porosity in Figure 4 and by comparing both PHIT (S) and PHIT (D) porosity values. However, they are less common than the channels. In some cases, the shells have been filled with sediment, and this is marked by the occurrence of geopetal structures (cf. Fig. 2, 2210 m of measured depth). The weakest components were fractured, as visible from a spiky MSFL curve (Fig. 4).

The impact of cementation was far less extensive in comparison to the other biofacies. However, the diversification of the precipitated phases is higher, as compared to the remaining subdivisions (see the "Cement stratigraphy" chapter above). Various forms of calcite and dolomite, often surrounding the voids are accompanied by poikilotopic anhydrite (e.g., Fig. 7B). The proportion of anhydrite and sparry calcite cements increases towards the bottom of the biofacies (Fig. 2). Anhydrite usually was precipitated within the bivalve and/or brachiopod shells, as was the drusy and less common sparry calcite (cf. Figs 7A, G, 8G, 9C).

The minimum total porosity from the log data is around 11%, as indicated by the sonic porosity PHIT (S), whereas the maximum value indicated by the PHIT (D) curve equals 32% (Fig. 4). The effective PHIE (LLS) porosity generally ranges between ca. 7% and 25%, with an average of ca. 16% (Fig. 4; Appendix). The average helium porosity is roughly 14%, with an average permeability of 23 mD (Fig. 6A; Appendix). The permeability varies between 0 and 134 mD (see Fig. 6A; Appendix). In places, the samples with a high proportion of channel porosity have slightly higher permeability values (see AR14, AR3, AR7, AM15 and AR5 samples in Appendix).

The stromatolitic biofacies

Typically for the region, the reef terminates upward with stromatolitic bindstones (Figs 8H, I, 10H) containing oncoids (cf. Figs 2, 3). The stromatolitic biofacies is developed differently in the two wells studied. In the case of the Brońsko-1 well, this division is characterized by generally low porosity values, yet remains moderately permeable. An average permeability value of ca. 20.2 mD was observed (Fig. 6A; Appendix). Locally, its values even can exceed 100 mD, others being close to 0 mD (Fig. 6A). The total porosity indicated from PHIT (S) and PHIT (D) curves starts from roughly 3%, reaching over 20% near the transition zone into the bryozoan-foraminifer biofacies (Figs 4, 6A). The PHIE (LLS) readings differ slightly; the porosity varies between ca 4% and 18%, with an average of 9.10% (close to the laboratory data – 9.24% – cf. Appendix; Figs 4, 6A). There is a weak relationship between porosity and permeability, with the R^2 of 0.47 (cf. Fig. 6A).

At the Brońsko-2 location, the stromatolitic layer is strongly dolomitized and contains numerous vugs and/or fenestral voids (Figs 10H, 11H). It is also cut by fractures in places. Calcite cements are common as well (see the "Cement stratigraphy" section above and cf. Fig. 8H, I). But even though the dolomitized top of the Brońsko-2 Ca1 section is more porous, this was modified to some extent by large amounts of sparry, poikilotopic anhydrite and sparry calcite filling the majority of the voids. Here, the geophysically derived total porosity – PHIT (S) and PHIT (D) – ranges between 3% and 10% (Fig. 5), while the effective PHIE (LLS) porosity appeared to change between 5% and as much as over 17% (the average of 14.21%, as opposed to ca. 11% from helium porosimetry – cf. Figs 5, 6B; Appendix). The permeability is extremely low and hardly ever exceeds 0.1 mD, with a maximum of just 0.7 mD, and an average value of 0.15 mD (Fig. 6B; Appendix). The fractures seem to be partially cemented, since both shallow and deep resistivity logs read higher at their suspected location (see zone 1 in Fig. 5).

INTERPRETATION AND DISCUSSION

The biofacies observed in the Brońsko Reef resemble those identified in other reefs of the region (cf. Dyjaczyński *et al*., 2001). An appropriate example concerns the Jabłonna Reef, described in sedimentological and diagenetic detail by T. M. Peryt *et al*. (2016). With slight differences, the biofacies considered also correspond to these recognized by T. M. Peryt *et al*. (2012), who presented an overview of the Polish Ca1 reefs. A main difference is that the *Horridonia* biofacies could not be distinguished as different genera of brachiopods were recognized in both of the wells studied, and *Horridonia* was not as abundant as for example in the Racot region (cf. Raczyński *et al*., 2016). A second difference is that the *Fenestella/Kingopora* biofacies was not subdivided since the fenestrate bryozoans, with few exceptions, were not as ideally and frequently preserved as in other reefs of the region. A similar situation was in the Bonikowo Reef, as reported by Raczyński *et al*. (2017), where delicate fenestrate bryozoans were preserved only sporadically.

The diagenetic sequences resemble those observed in other, locally occurring Ca1 reefs, where in particular cementation by polyphase dolomite and anhydrite was common (T. M. Peryt, 1984; Jasionowski *et al*., 2000; Dyjaczyński *et al*., 2001; Jasionowski *et al*., 2014).

Reconstruction of diagenetic history

The timing of specific diagenetic events is illustrated graphically in Figure 13. Early diagenesis probably started with calcite cementation taking place in a marine environment, since fibrous, bladed and equant calcite cements com-

---

cies showing large number of fenestrate bryozoans (moderate water energy), commonly encrusted by foraminifers. Also note the mouldic porosity (2202, B1). **H.** Stromatolitic biofacies – stromatolites and dolomitization-related vuggy porosity (2182, B2). The approximate depths of samples extraction are shown in brackets (measured depth; see Figs 2, 3). B1 – Brońsko-1, B2 – Brońsko-2.

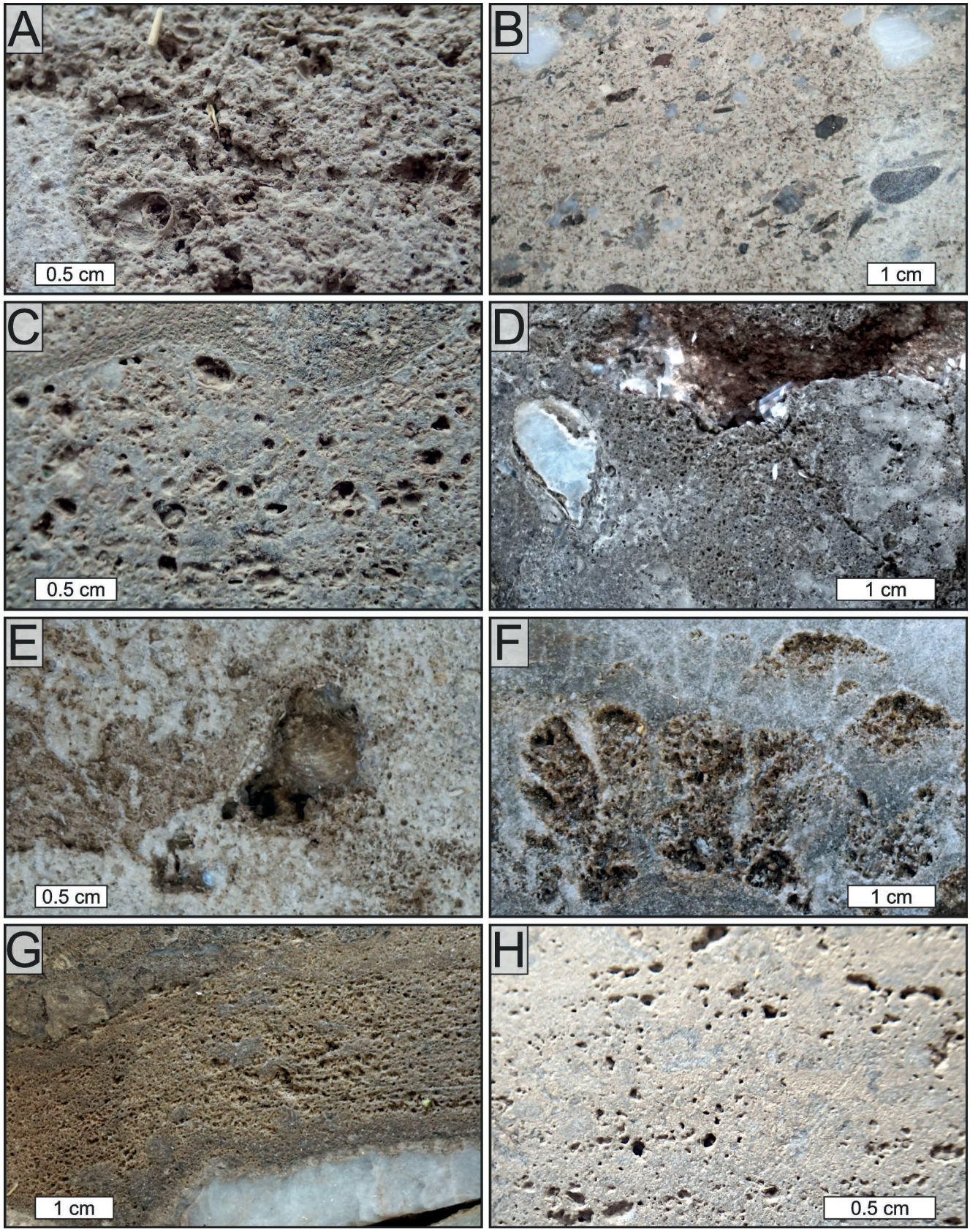

Fig. 11. Drill core photographs. **A.** The bottom of the bivalve-gastropod biofacies, gradually passing into *Acanthocladia* – well-preserved branches of bryozoans among the gastropod-related mouldic porosity (2193, B2). **B.** Extraclast- and anhydrite-rich, poorly porous horizon of the *Acanthocladia* biofacies (2244, B1). **C.** Local terebratulid brachiopod coquina developed in the bivalve-gastropod biofacies. Note the mouldic porosity and low admixture of anhydrite (2194, B2). **D.** Extensively cemented (anhydrite within the bivalve shells) but moderately fractured part of the bivalve-gastropod biofacies (2223, B1). **E.** Bivalve-gastropod biofacies showing a partially dissolved brachiopod shell (2188, B2). **F.** Brachiopod-bryozoan biofacies (transition to bryozoan-foraminifer) represented by shell material filled

monly rim the bioclasts. Calcite veins probably occurred owing to early, synsedimentary tectonics creating fissures that were subsequently filled with calcite (cf. Flügel, 2010).

The main diagenetic processes that impacted the strata investigated were dolomitization and dolomite and/or anhydrite cementation (cf. Jasionowski *et al*., 2000, 2014; Fig. 13). Jasionowski *et al*. (2014) concluded that the dolomitization patterns noted for the Wolsztyn Ridge reefs are too complicated for the exact timing and origin of individual events to be ascertained with certainty. He concluded that both early (sabkha and reflux) and burial dolomitization accounted for the alteration of the Ca1. According to the results obtained, it seems probable that the Ca1 strata of the Brońsko Reef was exposed to multistage reflux and sabkha episodes (chiefly the bivalve-gastropod and brachiopod-bryozoan biofacies), a possible seepage from the overlying Lower Anhydrite (PZ1, A1d) sulphates (mainly the bivalve-gastropod, bryozoan-foraminifer and stromatolitic biofacies) and burial conditions.

Particularly the chaotically distributed dolomicrite present in larger amounts in the bivalve-gastropod and brachiopod-bryozoan divisions seems to have been connected with a sabkha environment. This may be explained additionally by the common presence of chicken-wire and pile-of-bricks anhydrite in these sections. The former is believed to have formed as anhydrite laths progressively replaced the enclosing sediment (Aleali *et al*., 2013; Warren, 2016). Younger laths probably grew in an 'inside-out' manner between the previously formed crystals to ultimately give the impression of a chicken-wire texture (see Aleali *et al*., 2013; Abdioğlu *et al*., 2015 with references therein; Warren, 2016). The pile-of-bricks texture of some anhydrite crystals appears to indicate an early physical compaction, which acted on the anhydrite laths, resulting in breakage and fragmentation of them (Machel and Burton, 1991). Machel (2004) suggested that the pile-of-bricks fabric usually is not connected with gypsum replacement. Single lenticular gypsum crystals are present among the anhydrite and no clear pseudomorphs after the former were noted. Direct precipitation of anhydrite was possible in dry, periodically flooded sabkha areas (cf. Nusara *et al*., 2017). A sabkha also may be indicated by the nearly positive $\delta^{18}O$ values obtained for the dolomites by Dyjaczyński *et al*. (2001) and later by Jasionowski *et al*. (2014).

The imprint of sabkha conditions on the Ca1 strata to some extent also could have been controlled by the migration of dense brines from the overlying A1d deposits (T. M. Peryt, 1984; Jasionowski *et al*., 2014). Such a scenario also matches the co-existence of chicken-wire and lath-shaped anhydrite for the brachiopod-bryozoan biofacies. The latter in places occurs in the brachiopod caverns, which probably had been formed by fresh-water flushing (no evidence for karst), perhaps taking place after the formation of syndepositional (early sabkha) chicken-wire anhydrite, but before the precipitation of the burial, lath-shaped anhydrite (cf. Fig. 13). Common dolomicrite inclusions, observed within the poikilotopic, lath-shaped or even smooth-ended rosette anhydrite, also appear to be in accordance with the alteration of strata after burial (Nollet *et al*., 2005; Eggie *et al*., 2014). Since the presence of inclusions is even more common for the bryozoan-foraminifer biofacies, and the division generally lacks the chicken-wire or other early sabkha-related anhydrite fabrics, an interpretation is that the stromatolitic, bryozoan-foraminifer and the upper part of the bivalve-gastropod biofacies mainly underwent shallow-burial anhydrite cementation. Therefore, it seems probable that for the sections listed, dense A1d brines were responsible for the formation of most of the anhydrite. It is also possible that the horizons mentioned were dolomitized on this occasion, since the medium-crystalline dolosparite – more common in lagoonal settings (Machel, 2004) – is rather rare here, especially in the stromatolitic and bryozoan-foraminifer biofacies (cf. T. M. Peryt, 1984; Jasionowski *et al*., 2014). Thus, following dolomitization, anhydrite cement could have filled some of the dolomitization-related vugs present in the stromatolitic strata of the Brońsko-2 section. Machel (2004) explained such structures as dolomitization-related, since the rock fragments, including calcite-rich fossils are dissolved as an integral part of this process, ensuring the delivery of Ca ions. It is also highly probable that the vugs were accompanied by some proportion of fenestral porosity, connected with gas expulsion during the decay of organic matter (Hu and Huang, 2017). However, reconsidering the dolomitization, Machel (2004) observed that provided that low-temperature dolomitization takes place, the process will not destroy the primary rock texture (which is undamaged here), allowing the origin of the voids to be deciphered, for example the gastropod moulds. In addition, some vugs are still partially open, although many of them carry the signs of anhydrite cementation, which, according to Machel (2004) indicates that the vugs probably did not exist before the dolomitization. Another argument is that the matrix is still not fully dolomitized (see Machel, 2004). If the vugs had been created by meteoric dissolution, a karst surface would have been present in this layer. Vuggy dolostones also were described by other researchers, for example Fu and King (2010).

Some admixture of a medium-crystalline dolosparite is interpreted either as a reflux, on account of its fabric (see Machel, 2004) or as burial dolomite (cf. Jasionowski *et al*., 2014). The reflux model best fits the biofacies underlying the bryozoan-foraminifer biofacies. The reflux events might have taken place in a lagoonal setting (cf. Van der Baan, 1990; Becker and Bechstädt, 2006; Fig. 13), as discussed in more detail in the section "Water depth interpretation" below. Moreover, Mg-rich fluids could have migrated downwards to form isopachous dolomite rims in the *Acanthocladia* biofacies as a part of cementation process (cf. T. M. Peryt, 1984; Fig. 13).

---

with bryozoan detritus (2214, B1). **G.** Intraparticle porosity in the stromatolitic biofacies, probably of microbial origin (2196, B1). **H.** Stromatolitic biofacies – small dolomitization-related vugs (2183, B2). The approximate depths of samples extraction are shown in brackets (measured depth; see Figs 2, 3). B1 – Brońsko-1, B2 – Brońsko-2.

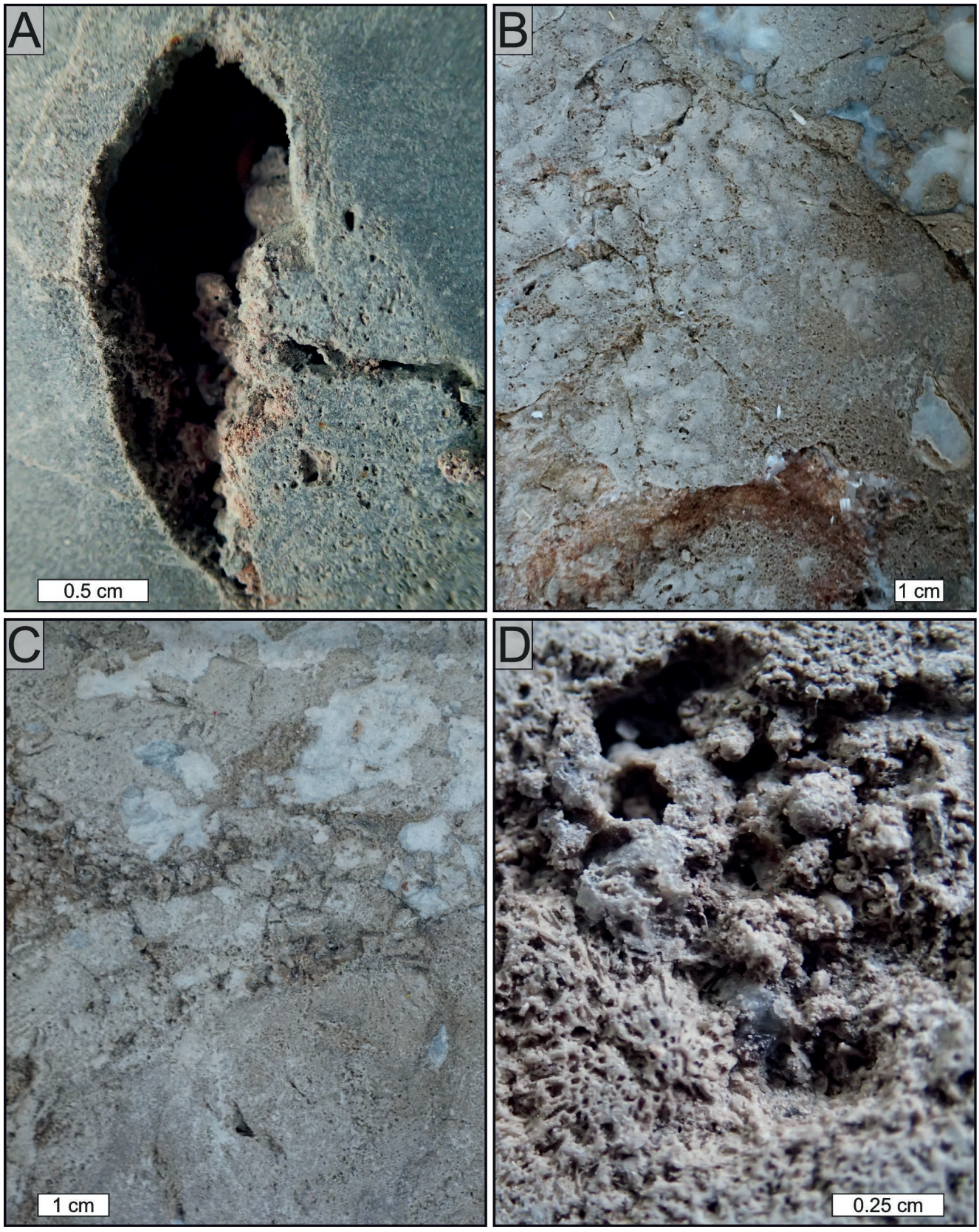

Fig. 12. Drill core photographs. **A.** Cavernous porosity surrounded by single fractures in the bryozoan-foraminifer biofacies (2207, B1). **B.** A well-organized system of fractures (resembling pseudokarren), co-occurring with cavernous porosity in the bivalve-gastropod biofacies (2223.1, B1). **C.** A strongly fractured interval of the bivalve-gastropod biofacies, showing partial brecciation of rocks (2222,9, B1). **D.** Mouldic, cavernous and intraparticle porosity within the bivalve-gastropod biofacies; note the encrusting bryozoans in the lower left corner of the image (2189, B2). The moulds are connected with small bivalves, ostracods and gastropods. The approximate depths of samples extraction are shown in brackets (measured depth; see Figs 2, 3). B1 – Brońsko-1, B2 – Brońsko-2.

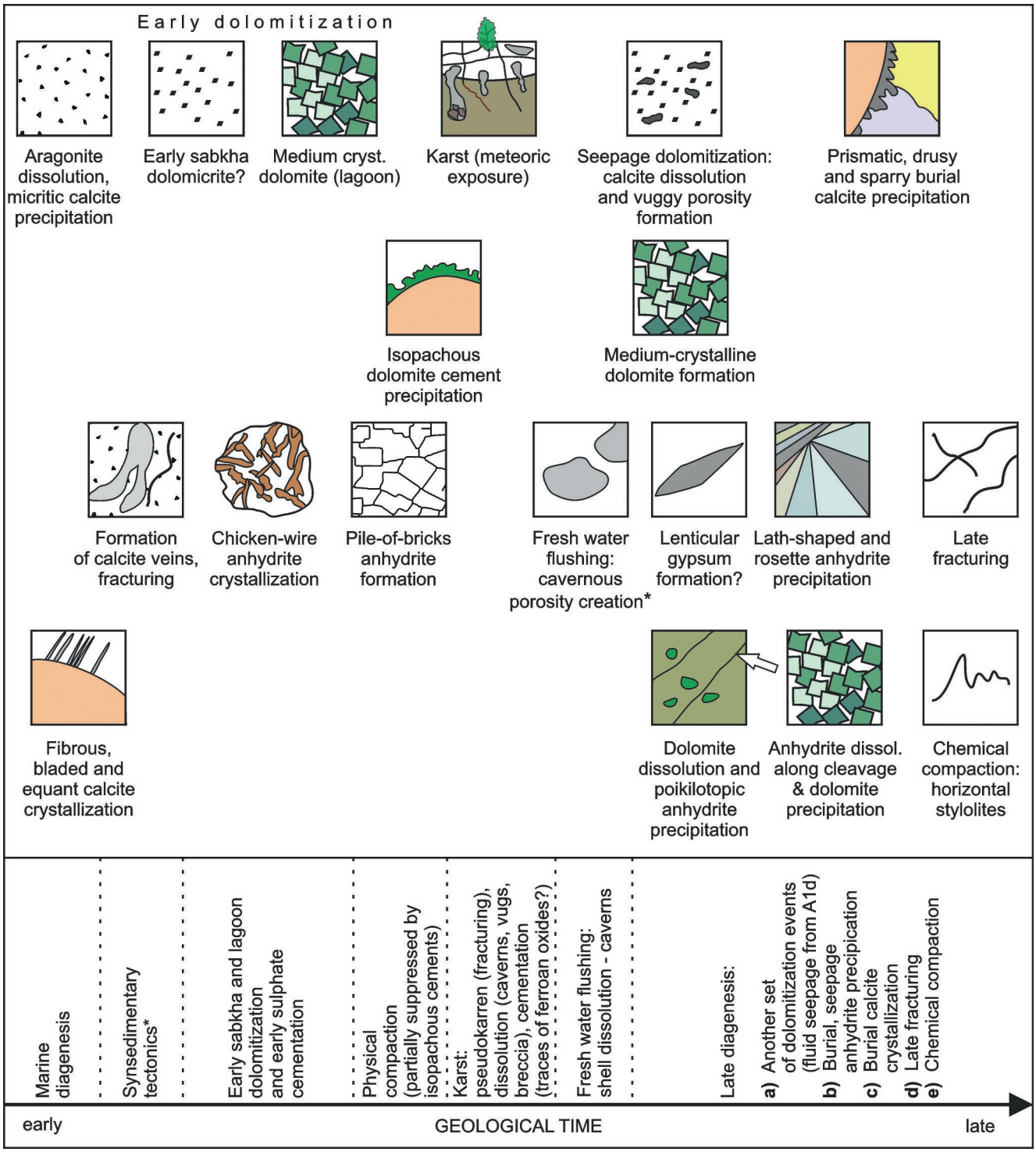

Fig. 13. A generalized scheme of diagenetic events impacting the strata of the Brońsko Reef. Note several episodes of dolomitization and dolomite cementation, the exact timing of which is hard to ascertain. Similarly, the sulphate cementation had a multistage character, but was intensified during the burial of the strata. * Note that synsedimentary tectonics might have been activated and suppressed at several different times, as was the fracturing and fresh water flushing. The majority of the ferroan oxides (and barite) are artificial, and probably come from the drilling mud, but traces of Fe-rich material also might have been connected with karst processes. White arrow schematically marks the cleavage of anhydrite, along which dolomite precipitated.

In a shallow, probably meteorically exposed setting (see the discussion below on sea-level changes), numerous vertical and horizontal fractures resembling small-scale karren or pseudokarren (Choquette and James, 1988; Desrochers and James, 1988; Kerans and Donaldson, 1988), were created and restricted to the upper section of the bivalve-gastropod biofacies. The suspected karst surface might be indicated additionally by the common presence of breccias, vugs and large caverns (cf. T. M. Peryt, 1984; Demicco and Hardie, 1994). However, the absence of vadose cements provides a counter-argument. Perhaps they were fully recrystallized to drusy or sparry burial calcite, during later diagenetic stages (see Fig. 13; Jasionowski *et al*., 2000, 2014; Fheed *et al*., 2015). Also, neptunian dykes occur in the upper parts of the bivalve-gastropod and bryozoan-foraminifer biofacies, but these are not indicative of karst, since they might have originated in several different depositional settings, including the marine environment, as concluded by Flügel (2010). It should be added that although the deposition of very limited amounts of red clay containing ferroan oxides might have taken place during the suspected meteoric exposure, most of the red material is artificial and probably comes from the drilling mud, since it contains a large admixture of barite and preferentially fills larger cavities or fractures.

As a result of continuing burial, another generation of dolomite appeared and began to replace the anhydrite along its cleavage surfaces (Fig. 13). Evidence for the burial conditions, under which part of dolomite probably formed, also was given by Jasionowski *et al*. (2014), who observed some calcitization of dolomite crystals, and their co-occurrence with saddle dolomite. In the case studied, the apparent burial dolomites have medium-crystalline, subhedral fabrics, and are widespread, particularly in the lower part of Ca1. Here it is also noteworthy that some samples have an obliterated texture, probably due to the activity of the burial fluids (see Machel, 2004).

The medium-crystalline dolosparite was followed by sparry, burial calcite cement that probably was formed at a similar time as the drusy and also well-developed, prismatic calcite crystals, filling the pore spaces (see Fig. 13; Tucker and Wright, 1990; T. M. Peryt *et al*., 2012). Finally another set of fractures and horizontal stylolites were formed, and this probably happened during the later stages of burial (see Fig. 13). These commonly cut the older cements discussed above.

Factors controlling reservoir quality increase

Among all the processes discussed, the greatest porosity increase – particularly for the bivalve-gastropod biofacies – was ensured by meteoric dissolution, providing vugs, caverns, and well-organized fractures. It is also probable that the bryozoan-foraminifer biofacies was temporarily exposed meteorically, but clear evidence for this is lacking (see the ongoing discussion).

Another process responsible for porosity gain was polyphase dolomitization. Here the dolomitization-related vugs and a number of intercrystalline pores can be listed. The first episode of dolomitization particularly enhanced the matrix-related microporosity. The subsequent stages of the dolomitization, leading to the formation of the medium-crystalline dolosparite, were not effective in porosity gain and even to some extent reduced the porosity as a part of the cementation process. However, the presence of isopachous rims of calcite or dolomite acted against physical compaction, thus preventing further porosity loss (Moore and Wade, 2013).

Factors controlling reservoir quality decrease

Porosity was destroyed mainly by anhydrite cementation that filled the majority of previously available vugs and caverns. The early chicken-wire anhydrite and the burial lath-shaped and rosette anhydrite (cf. Nollet *et al*., 2005) also account for a decrease in porosity and permeability. The greatest decrease in porosity concerns first of all the sabkha-related top of the bivalve-gastropod biofacies and to some extent also the overlying brachiopod-bryozoan biofacies, where the infiltration of dense A1d brines probably enhanced anhydrite precipitation.

Similarly, a range of calcite cements filled the available pore spaces. Sparry burial calcite (cf. Jasionowski *et al*., 2014) should be mentioned here, as it significantly reduced the porosity and permeability of the bryozoan-foraminifer biofacies. This kind of cement also was found in the early fractures, and thus appeared to worsen porosity-permeability relations (low R^2 coefficient). Lastly, chemical compaction leaving an impermeable residue accounted for considerable permeability decrease.

Water depth and energy reconstruction

The general trend of the sea-level changes was typical for the SPBA, and especially for the Polish part of the basin (T. M. Peryt, 1984; Pikulski and Wolnowski, 2005). In the case studied, the sea-level changed twice, with two marked drops in water level. These were the result of both active tectonic subsidence (Kiersnowski *et al*., 2010) and glacially controlled eustatic changes (T. M. Peryt, 1984; T. M. Peryt *et al*., 2016). The salinity of the water was normal, as shown by numerous crinoids occurring in the Ca1 strata (cf. Raczyński, 2000; Dyjaczyński *et al*., 2001; Scholle and Ulmer-Scholle, 2003; Pikulski and Wolnowski, 2005). The general changes in sea level can be inferred from: (1) associations of organisms, preferring particular water depths, (2) sedimentary structures, such as stromatolites, (3) the cement fabrics, and (4) karst features, indicating the meteoric exposure of strata.

For a reconstruction of the relative sea-level fluctuations, the *Acanthocladia* biofacies is discussed first. The water must have been moderately deep, as the branched bryozoans – typically inhabiting the region close to the storm wave-base (T. M. Peryt *et al*., 2016) – are common. However, T. M. Peryt *et al*. (2016) noted that the water depth was changing from shallow to deep at that time, probably owing to storm wave-base fluctuations. This explains the significant fragmentation of the bryozoan anceps. In the case of the Brońsko-2 well, the *Acanthocladia* biofacies shows the signs of an even shallower environment, since its deposition started on a tectonically uplifted Carboniferous block (Dyjaczyński *et al*., 2001; Pikulski and Wolnowski, 2005; Kiersnowski *et al*., 2010).

After the substrate was colonized by the *Acanthocladia* bryozoans, the water became deeper, allowing for the appearance of the bivalve-gastropod biofacies, preferring greater water depths, which probably developed at the reef core (T. M. Peryt *et al*., 2016). The energy of water was rather calm this time, since the bivalves, gastropods, and the *Dielasma* brachiopods – also observed in the Jabłonna Reef (T. M. Peryt *et al*., 2016) – are preserved without major damage (cf. Scholle and Ulmer-Scholle, 2003). Later, this contributed to the formation of cavernous porosity due to the dissolution of shell material (cf. Fheed *et al*., 2015, 2018).

The deepening of the water is interpreted as a consequence of active tectonics and/or thermal subsidence acting with an overall, relative rise in sea-level (Kiersnowski *et al*., 2010; cf. Pharaoh *et al*., 2010). Favourable conditions allowed for reef aggradation. When the reef approached the surface, one could expect a significant increase in water energy, but instead laminations indicative of calm conditions appeared (see Van der Baan, 1990). Therefore, a backreef setting is assumed to have developed, protected against wave action by a distant reef margin, until approaching the sea-level, as marked by microbial structures (cf. Hollingworth and Pettigrew, 1988; T. M. Peryt *et al*., 2016). The back reef is a favourable setting for bivalves, being mostly infaunal or epifaunal organisms (Raczyński *et al*., 2017). At this time, probably some of the dolomite was formed by brine reflux, because it shows a clearly developed, medium-crystalline fabric and could have been created in the presence of a barrier that might have been crossed regularly by Mg-rich marine waters promoting dolomitization (cf. T. M. Peryt, 1984; Machel, 2004). It is possible that continuous aggradation of the reef led to the formation of sabkha conditions, evidenced by the abundance of chicken-wire and pile-of-bricks anhydrite and the slightly positive $\delta^{18}O$ values observed by Dyjaczyński *et al*. (2001) and Jasionowski *et al*. (2014). It is noteworthy that dense brines migrating through the Ca1 strata added some imprint to the pre-existing situation (see the above discussion on diagenesis).

As the reef continued to grow, it ultimately was exposed to meteoric dissolution, evidenced by multiple karren-like fractures and widespread caverns. T. M. Peryt (1984) and T. M. Peryt *et al*. (2012) recognized the meteoric exposure of the reefs of the Brońsko region, but interestingly tied it with the *Fenestella*/*Kingopora* biofacies, an equivalent of the bryozoan-foraminifer biofacies. However, the latter shows much weaker signs of potential exposure than the bivalve-gastropod biofacies, occurring just below the stromatolitic biofacies of the Brońsko-2 section.

Next, the relative sea-level generally rose again (cf. T. M. Peryt *et al*., 2016) as the brachiopod-bryozoan biofacies started to develop. But the rate of the tectonic subsidence (Kiersnowski *et al*., 2010) probably was not enough to submerge the uplifted block at the location of the Brońsko-2 well, where a break in deposition probably lasted until the formation of the stromatolitic layer in both of the wells studied.

The brachiopod-bryozoan biofacies consisted of abundant terebratulid (typically *Dielasma*) and strophomenid brachiopods, accompanied by bryozoans. Brachiopods are epifaunal organisms, commonly inhabiting relatively deep or moderately deep settings (Raczyński *et al*., 2017). The stage of the relatively deep-water conditions additionally may be corroborated by the common presence of marine, equant and/or fibrous cements, discussed above. Some of the brachiopods, still showing their spines, managed to survive, thus indicating a relatively calm, protected environment of deposition (Scholle and Ulmer-Scholle, 2003; Raczyński *et al*., 2017). As a result, the large brachiopod and bryozoan shells and skeletons could have been maintained and later were dissolved to a major extent (Fig. 14).

Later, perhaps owing to ongoing evaporation and the limited rate of subsidence, the water level dropped slightly, allowing dolomitization and sulphate cementation. The conditions here were analogous to these previously described for the bivalve-gastropod biofacies, but no evidence for meteoric conditions exists in this case.

As tectonic subsidence continued (cf. Kiersnowski *et al*., 2010), the system returned to marine conditions. At this time, the bryozoan-foraminifer biofacies was deposited at the Brońsko-1 well location. This biofacies serves a textbook example of Zechstein fossils, the anatomy and characteristic features of which were discussed comprehensively by Hollingworth and Pettigrew (1988). The division is chiefly represented by different bryozoan genera (cf. Hara *et al*., 2013), frequently encrusted by foraminifers and small ostracods. They are accompanied by numerous gastropods, bivalves and less common brachiopods. The growing proportion of fenestral bryozoans, especially towards the top of Ca1, is interpreted as the product of a proceeding shallowing of water, due to aggradation of the reef (see T. M. Peryt *et al*., 2012, 2016; Raczyński *et al*., 2017).

Finally, the reef clearly reached the surface, probably because of continuous aggradation and a significant relative fall in sea-level, described for example by T. M. Peryt (1984) and Weidlich (2002). Consequently, the extremely shallow-water stromatolitic biofacies was deposited at both studied locations (cf. Karaca, 2015; Warren, 2016).

The stromatolites typically terminate the reef successions of the region (see Dyjaczyński *et al*., 2001; T. M. Peryt *et al*., 2016). However, Fheed *et al*. (2015) noted a very rapid decrease in sea-level for the isolated part of the Wielichowo Reef that did not allow deposition of the stromatolitic layer. Perhaps, this was a consequence of active tectonics (cf. Kiersnowski *et al*., 2010). In contrast, in some cases in the Zechstein, stromatolites of different kinds appear to have been the sole or predominant component of a reef, along with coated grains. Paul (1980), for instance, described a strongly dolomitized stromatolite-dominated buildup in the Harz Mountains, Germany. Smith (1986), in turn, noted what he called "the Trow Point Bed", which was the uppermost Ca1 interval, dominated by coated grains and stromatolites, occurring at some basinal localities of the English Zechstein. The strata in this interval were very tightly packed, without any voids, and exhibited signs of stylolitization, also common in the studied case. It used to contain sparsely distributed fossils, including bivalves, bryozoans, and crinoids. The bed described was also found to have been dolomitized to a significant extent – as in the case of the Brońsko-2 section, where numerous vugs were created in this way (cf. Machel, 2004).

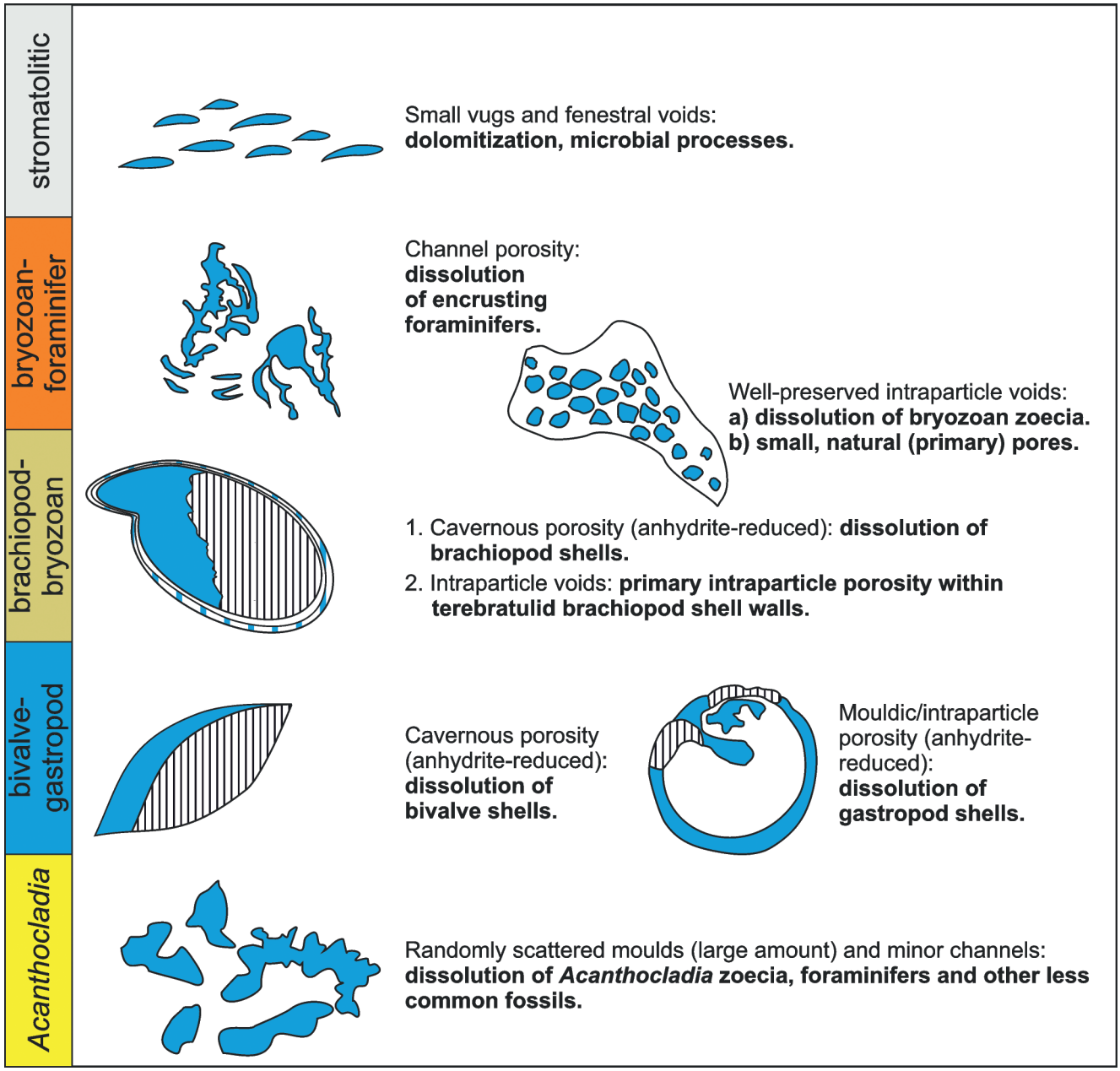

Fig. 14. Summary of major porosity types encountered in the Brońsko Reef. The related processes (origin) are presented in bold. Blue/black denotes porosity, white indicates undissolved bioclast fragments, while dashed filling marks anhydrite cement. Biofacies are presented on the left. Note that the intraparticle porosity in the case of bryozoans might be either of primary or secondary origin. For more pore types see Figs 8–12.

The relations between sedimentation and porosity/permeability evolution

The *Acanthocladia* biofacies

The presence of *Acanthocladia* in the lowermost parts of Ca1 is very common in the region. T. M. Peryt *et al*. (2012) observed numerous branched bryozoans, frequently co-occurring with brachiopod shells (chiefly *Dielasma*), bivalves (e.g., *Bakevellia, Liebea*), gastropods, crinoids, and foraminifers, appearing within the biofacies. The *Acanthocladia* biofacies also was noted in the Bonikowo (Raczyński *et al*., 2017), Jabłonna (T. M. Peryt *et al*., 2016) and Wielichowo (Fheed *et al*., 2015) reefs. Moreover, T. M. Peryt *et al*. (2012) drew attention to the presence of many moulds, left after the solution of either bryozoan zoaria or brachiopod shells (cf. Fig. 14). In the case of the Brońsko-2 section, the proportion of mouldic porosity increases abruptly owing to the dissolution of numerous gastropod shells, particularly common in the bivalve-gastropod biofacies. The dissolution probably took place under conditions of burial, as no indication of a karst surface exists for the *Acanthocladia* biofacies.

The encrusting bryozoans surrounded the bivalve shells, together forming even more moulds and vugs. The bryozoan zoaria were greatly fragmented (Fig. 14), thus reducing the sizes of the potentially available moulds and intraparticle pores (cf. Raczyński *et al*., 2017). Therefore,

the connectivity of the pore spaces is questionable, giving an average permeability value even below 1 mD, in the case of Brońsko-2 strata. In places, where scattering was weaker, the moulds evolved into narrow dissolution channels formed owing to the amalgamation of bryozoan- and/or foraminifer-related voids. These also were supported by the bivalve-related caverns. Probably this explains the better permeability of *Acanthocladia* biofacies in the Brońsko-1 section. However, such channels are much less common than those present in the bryozoan-foraminifer or even in the bivalve-gastropod biofacies, discussed below. In addition, the related weakening of the material probably promoted the propagation of tectonic fractures, generally common in both wells studied. In the Brońsko-2 section, however, some fractures were cemented with anhydrite, as indicated by thin section examination and resistivity logs that give higher readings in such places.

Despite poor permeability, moderate effective porosity and practically non-existent porosity-permeability relations, the *Acanthocladia* biofacies is still one of the most porous horizons studied. This is due to two different situations: (1) a large number of pores related either to fragmented bryozoan zoecia or the dissolved shells of foraminifers; and (2) a relatively low amount of anhydrite cement (mostly of burial origin – see Fig. 13). In the case of the Brońsko-2 section, the dolomitization was more intensive, but the intercrystalline pore network was still not a site of increased permeability, which does not exceed 10 mD, according to the data gathered. From a petrophysical point of view, the admixture of clay minerals is negative and this impacts on the GR log, and thus the calculated shaliness. All these features seem to have resulted directly from the proximity of the Pre-Zechstein basement, from which numerous extraclasts containing clay minerals, quartz, and tight clastic rock fragments had been detached, thus generally decreasing the fluid flow and storage capability.

According to other researchers, the lowermost part of this biofacies also is characterized frequently by the presence of breccias (see Smith, 1970; cf. T. M. Peryt *et al*., 2012). Smith (1972) described English collapse breccias, believed to have formed because of the dissolution of sulphates and nearly simultaneous dedolomitization, which also destabilized the rocks. Smith (1970) also reported gravitational breccias, for example formed by submarine slumping. Such phenomena do not seem to match the situations observed in Poland. T. M. Peryt *et al*. (2012) neglected gravitation-related processes as potentially being responsible for the brecciation of the Polish Ca1 rocks and explained that instead it should be considered as a Transgressive System Track (TST) sediment (cf. Dyjaczyński *et al*., 2001). Regardless of the origin of similar breccias, both poor sorting and the tight character of such strata make them petrophysically unattractive in terms of their reservoir potential.

The bivalve-gastropod biofacies

In terms of its main components – chiefly *Bakevellia* and *Liebea* bivalves, accompanied by extremely numerous gastropods of different genera – this division is similar to the *Bakevellia/Liebea* biofacies, distinguished in the reefs of West Poland by T. M. Peryt *et al*. (2012). Such biofacies also were observed to be common in England (Hollingworth and Pettigrew, 1988; Smith, 1986, 1995 with references therein) and Germany (Kerkmann, 1969; Füchtbauer, 1980).

The biofacies occupies a considerable part of the Ca1 section – for the Brońsko-2 well as much as three quarters of the Ca1 profile. In both cases, it is one of the most porous horizons studied. The existence of little fragmentation of the mineralogically unstable fossils raised the probability of an extensive dissolution. Cementation is generally stronger in the Brońsko-1 section, which can be confirmed from the well logs and especially from the local maxima of the DT logs. Because most of fossils encountered are bivalves and gastropods – with a minor admixture of brachiopods – they can be considered as potentially dissolution-prone material that was formerly composed of aragonite (see Walter, 1985; Scholle and Ulmer-Scholle, 2004; and cf. Figs 10B, 14). Despite this, some of the bivalve shells exhibit a well-preserved, prismatic structure, indicating their calcitic origin and lower susceptibility to dissolution (cf. Harris *et al*., 1985). However, taking into account the complicated combination of structural defects, mineral stability, and other factors controlling the dissolution rate, such exceptions seem to be rather insignificant. This is discussed in more detail in the bryozoan-foraminifer biofacies subsection (see below), where Walter's (1985) theory about a strong correlation between structural defects in a shell and its dissolution susceptibility is considered.

The porosity is generally high, and commonly exceeds 15%, specifically in the case of the Brońsko-2 section, but the differences between the helium porosimetry and the geophysically derived porosity, represented by the PHIT (S) and PHIT (D) values, are significant. This implies that the heterogeneity in the distribution of the bivalve-related caverns is considerable. However, on a reservoir scale, small shifts between the caverns are negligible and a relatively "high" permeability of approximately 20 mD might have facilitated shell dissolution. In the Brońsko-1 section, the permeability was improved by dolomitization, but then reduced by sulphate cementation, while in the Brońsko-2 sequence, the rocks were dolomitized subordinately, although they were cemented less extensively with anhydrite. This seems to explain the similar permeability trends in the two cases. However, a sound correlation between porosity and permeability is striking in the context of the common presence of anhydrite cements. In the opinion of the author, this is due to both early and late diagenetic fracturing as well as to further dolomitization (Fig. 13), together ensuring a continuous dissolution of the mineralogically unstable bivalve shells. However, the porosity locally could have been decreased owing to a large amount of carbonate mud and a tightly packed dolomite mosaic, as was observed for lagoonal strata by Van der Baan (1990).

Lastly, it is necessary to consider the strong imprint on this biofacies left by meteoric exposure. Pseudokarst structures, resembling small-scale karren and vugs, originated at this stage (cf. Choquette and James, 1988) and some of them remained unfilled. On the other hand, many fractures were cemented entirely, often with anhydrite and calcite, increasing the resistivity log readings (Luthi, 2013) and lowering the permeability of the strata.

The brachiopod-bryozoan biofacies

Despite a large amount of anhydrite filling the pore spaces, large, open caverns were observed occasionally in the brachiopod-bryozoan biofacies (Fig. 14). It seems probable that they are connected with the former shells of terebratulid brachiopods that were surrounded by bryozoans (cf. Raczyński *et al*., 2017). Since there is no evidence for the meteoric exposure of this biofacies, the model of occasional fresh-water flushing through the system of fractures perhaps might explain the origin of the caverns (cf. Moore, 1989). It is noteworthy that in some cases, the shells of terebratulid brachiopods still exhibit some natural voids, oriented at right angles to the shell boundaries. They may be understood as primary intraparticle porosity (cf. Scholle and Ulmer-Scholle, 2003). It is probable that the isopachous dolomite rims (cf. Fig. 13) to some extent helped to save them from destruction by the proceeding mechanical compaction.

As proved above, at some stage in the deposition of the biofacies, the relative sea-level was falling. Microbial structures were developed and later dissolved to account for the formation of intraparticle porosity, together with that associated with dissolved bryozoan and bivalve fragments (Fig. 14).

Anhydrite cementation dramatically decreased the porosity of the biofacies. Thus, the porosity-permeability trend line only gives an R^2 coefficient of 0.45. Besides anhydrite cementation, this may also be related to the chaotic precipitation of burial calcite. The exact conditions, under which such cement originates have long been the subject of debate, but the source for its precipitation frequently is related to the downward migration of Ca-rich fluids (Tucker and Wright, 1990). Thus, probably when the readily soluble brachiopod shell material was dissolved and later saturated with such fluids, extensive precipitation of burial calcite and anhydrite could have reduced the pore space severely (see Fig. 13). Burial diagenesis affecting the Zechstein strata also was outlined by Clark (1986), who considered its role in reducing the porosity. Clark (1986) also noted large amounts of burial anhydrite filling the pore spaces. A similar situation has taken place for the Brońsko Reef, where widespread, burial, lath-shaped and rosette anhydrite are present (Fig. 13; cf. Nollet *et al*., 2005).

The bryozoan-foraminifer biofacies

The bryozoan-foraminifer biofacies was recognized only in the Brońko-1 section. A large amount of geometrically diversified pores is believed to be linked with the extraordinary variability of the original biota. Rich assemblages of fossils, including bryozoans, foraminifers, gastropods, bivalves, ostracods, and less common brachiopods, were equated with differences in the mineralogical composition of their shells and skeletons (Scholle and Ulmer-Scholle, 2003). T. M. Peryt (1984) noted that the leaching of the upper part of Polish Ca1 strata was selective. While most of the bryozoan zoaria usually are composed of calcite, typically low-magnesian calcite, the shells of foraminifers contain either high- or low-magnesian calcite. The ostracods can represent a combination of chitin and calcite (Scholle and Ulmer-Scholle, 2003). According to Scholle and Ulmer-Scholle (2003), the bivalves and gastropods usually are purely aragonitic, while brachiopod shells are composed mainly of low-magnesian calcite, with traces of aragonite. Walter (1985) noted that, ideally, the magnesian calcite would have been more soluble than aragonite, whereas the latter dissolved more easily than the low-magnesian calcite. This perhaps would explain why the bivalve shells were dissolved such extensively in the reef to form cavernous porosity. But on this occasion, it should be outlined that the bryozoan zoaria were dissolved – at least in most cases – to a large extent, as well. Importantly, it seems that the degree of the fragmentation of the fossils played a major role in the evolution of the porosity. Although the remains of both ostracods and foraminifers are expected to be less soluble than the bryozoan components, their shells typically are much smaller and less resistant than the bryozoan fragments, and therefore may contain more structural defects such as microfractures. This is related to Walter's (1985) conclusion that such structural defects can have a role in the process of dissolution as significant as the part played by skeletal mineralogy. This theory – though at the first glance, slightly questionable – answers the question as to why the high diversity of fossils might have promoted stronger dissolution in the case studied. Because the bryozoan zoaria in places were covered entirely by encrusting foraminifers and/or ostracods, they could have been ideal material for dissolution, even comparably to the aragonitic bivalve shells, more often encountered in the bivalve-gastropod biofacies. The more soluble fossils could have been dissolved to form new pathways for fluid flow, helping in the dissolution of the less soluble phases. This fits the presence of foraminifer-related dissolution channels. Foraminifers are a common constituent of Polish Ca1 reefs, and were recognized at many localities (e.g., Dyjaczyński *et al*., 1997; T. M. Peryt *et al*., 2012; T. M. Peryt and D. Peryt, 2012). A combination of the phenomena mentioned probably promoted a porosity increase within the bryozoan-foraminifer biofacies, today characterized by excellent reservoir parameters, except for the moderate permeability of some horizons.

After the death and fossilization of the bivalves, some bryozoans could have attached themselves to the bottom. They probably in turn became the sites of encrustation and ongoing fossilization. While the bivalve shells were dissolved to create relatively large caverns, the bryozoans together with the co-occurring organisms provided the locations for large amounts of intraparticle and mouldic porosity (Fig. 14). Some proportion of the primary intraparticle porosity also occurs between the fossilized bryozoan zoecia. This mainly concerns both the branched and columnar bryozoans present in the biofacies discussed (cf. Hu and Huang, 2017). The fenestrate genera could have provided even more space for dissolution, if they were not crushed during the increases in water energy of short duration deduced from the presence of some rudstone intercalations.

Encrustations around bryozoans frequently were observed by other researchers (cf. Smith, 1986; Taylor and Wilson, 2003; D. Peryt *et al*., 2012; T. M. Peryt *et al*., 2012; T. M. Peryt and D. Peryt, 2012; Raczyński *et al*., 2017). Peryt and Peryt (2012) reported foraminifer encrustations in North Poland and D. Peryt *et al*. (2012) recorded such occurrences in the Brońsko Reef. Although the organisms

frequently were the first ones to colonize the bottom of the forming Ca1 after a rapid transgression (cf. Dyjaczyński *et al*., 2001), according to the material studied, they were more common in the calmer waters of the bryozoan-foraminifer biofacies. They had an important impact on the evolution of mouldic porosity and later channel porosity. The foraminifer-related encrustations were perhaps the most important factor controlling gains in porosity/permeability within the biofacies considered (cf. Appendix 1; Fig. 14). The horizons with abundant encrustations were investigated petrophysically by means of NMR by Fheed *et al*. (2018) and later by Fheed and Krzyżak (2018). The authors detected numerous moulds and channels related to these features, as well as elongated caverns, probably left after bivalves. More details regarding the NMR results are given in the NMR subsection below. Unfortunately, the great petrophysical potential of this biofacies was reduced somewhat by the cementation involving both marine fibrous calcite and sparry burial calcite, discussed earlier (Fig. 13). Although at first glance it seems that the permeability is rather moderate or low (about 20 mD on average again), some samples containing dissolution channels have slightly higher permeability, reaching up to approximately 100 mD (Appendix 1). The poor porosity-permeability relationship (R^2 of 0.40) is probably due to polyphase cementation that took place mainly during a probable downward seepage of the Lower Werra Anhydrite brines.

Lastly, from a sedimentological point of view, the relatively strong fragmentation of the fenestrate bryozoans – typically inhabiting calm waters (T. M. Peryt *et al*., 2012) – is noteworthy. Naturally, less severe fragmentation increases the chances for porosity development. The considerable fragmentation of the fenestrate bryozoans might be explained by the possible reworking and/or transportation of the material. Perhaps this is why they cannot be tracked as frequently as for other objects, such as the isolated Wielichowo Reef (Fheed *et al*., 2015) or the Jabłonna Reef (T. M. Peryt *et al*., 2016).

In summary, the bryozoan-foraminifer biofacies seems to be an excellent reservoir horizon, as deduced from the high porosity and variability of pore types, high pore connectivity (channels), and relatively low anhydrite amount found within this division. However, the permeability is rather low, as discussed above.

The stromatolitic biofacies

It is to be expected that extremely shallow water most often promotes intensive cementation, including anhydrite precipitation and the general destruction of porosity (cf. Harris *et al*., 1985; Smith, 1986). This generally happened – at least for some layers of this biofacies. At the first glance, only minor fracturing events detectable on the resistivity logs were capable of slightly increasing the permeability for single horizons, but still this parameter often oscillated around 0 mD. On the other hand, limited dissolution of scarce fossils, such as small ostracods, foraminifers, and gastropod shells dispersed among the microbialites, gave rise to scattered mouldic porosity. But despite this, the porosity (at least for the strata of the Brońsko-1 section) remains relatively low. In the neighbouring Brońsko-2 section, the stromatolitic biofacies appeared to contain small vuggy voids, observable on the DT readings (cf. Figs 13, 14). These increased the porosity, but because of the limited connectivity of such structures, the permeability still remained very low. The higher average porosity in the case of the Brońsko-2 section, in the opinion of the author, results from much more intensive dolomitization. The dolomitization substantially enhanced the porosity and controlled the formation of the vuggy structures discussed above.

Regardless of this, the Zechstein stromatolites rarely appeared to show attractive petrophysical parameters owing to both physical and chemical compaction and intensive cementation. Because of this, the permeability of such horizons, especially when they lack fractures or contain healed fractures (see Fig. 5), also seems to be questionable. Poor porosity and permeability of the stromatolitic biofacies especially fits the situation in the Brońsko-1 well (cf. Smith, 1986), where poikilotopic anhydrite and tightly packed microbial structures did not allow for many voids to be developed and/or preserved.

When studying the Main Dolomite (Ca2) strata of North Germany, Steinhoff and Strohmenger (1996) also observed that large amounts of algal laminations typically influence the porosity in a negative manner. However, the authors mentioned that quite the opposite happens in the presence of numerous coated grains. In particular, the intercrystalline porosity was observed between the pellets, whereas the intraparticle porosity was found to be linked to oncoids and ooids with cortex-related microporosity. Finally, Steinhoff and Strohmenger (1996) noticed the role of fracturing in increasing the porosity of the stromatolitic layers, which fits the results obtained in this paper (Brońsko-1). The amount of coated grains seems to be moderate, or even relatively low, in the case of the Brońsko Reef. No significant influence of their presence on porosity was noted.

Nuclear magnetic resonance and X-ray microtomography in Ca1 porosity assessment

Several comments can be made about the Ca1 pore geometries of the Brońsko Reef studied by Fheed *et al*. (2018) by means of both μCT and NMR. Firstly, it was proved that the bryozoan-foraminifer biofacies often contains elongated caverns or massive mouldic/cavernous enclaves (cf. Fheed and Strzelecki, 2017; Fheed *et al*., 2018). It also was observed that the moulds frequently evolved into narrow dissolution channels, which were much more common than the caverns (cf. Figs 2, 3, 14; Fheed *et al.*, 2018). The channels were most numerous for the rocks from the Brońsko-1 well. The amount of typical vuggy porosity, in turn, is limited in the case studied, as compared for example to the isolated part of the Wielichowo Reef, subjected to low-field NMR analyzes by Fheed *et al*. (2015).

The dissolution channels were investigated thoroughly in the work of Fheed and Krzyżak (2018), where the authors employed diffusion-weighted NMR imaging (DWI) to resolve their geometry. High tortuosity of the system was observed, and the permeability varied around 100 mD. The main trend of the channel system was slightly angled from

vertical axis of the sample, which was taken perpendicularly with respect to the longest axis of the well. This was deduced on the basis of employing three mutually perpendicular magnetic field gradients, allowing for a nearly 3D assessment of the pore space. Such an approach enabled prediction of the direction of fluid inflow into the well, which, in the case studied was almost horizontal. Moreover, the dissolution channels also were observed on both μCT and high-field NMR images studied by Fheed *et al*. (2017), where the authors attempted to locate fossil-related voids and assess their contribution to porosity/permeability enhancement. Despite some role of ostracods in the formation of channel porosity, the detailed research performed in this article revealed that the channels are mostly foraminifer-related.

Both brachiopod-bryozoan and bivalve-gastropod biofacies appeared to be extensively cemented, as marked either by the zones devoid of water (NMR) or increased density (μCT; Fheed *et al*., 2017; Fheed *et al*., 2018; Fig. 14). For instance, the anhydrite-cemented zones had X-ray radiation absorption values exceeding 150, whereas the values used for porosity thresholding ranged between 0 and 93. The recognition of such zones was facilitated significantly by the utilization of a high-field NMR, working perfectly for rocks lacking (or containing little admixtures) of ferromagnetic phases, such as carbonates. Fheed *et al*. (2017), for instance, showed the high-field NMR images representing the partially anhydrite-filled bivalve shells, also observable in μCT pictures. The cementation intensity also was proved to correlate with an increased fluctuation of the low-field NMR signal, as concluded earlier by Fheed and Krzyżak (2017), in their study of the Wielichowo Reef rocks using relaxometric techniques.

Only a single, brecciated horizon of the *Acanthocladia* biofacies was probed and expectedly this exhibited low porosity (see Fheed *et al*., 2018). Moreover, cemented channels were observed in this interval.

Finally, the samples from the Brońsko-2 well exhibited a large number of moulds and fractures. Mouldic porosity was recognized as the most common porosity type in both wells (see Fheed *et al*., 2018). Fheed and Strzelecki (2017) took into consideration the geometry of pores, regarding the Ca1 of the Wielichowo Reef. The authors utilized μCT data and concluded that the original biota had a serious impact on the final character of the porosity. They noted that the fenestrate bryozoans, as compared to the branched (*Acanthocladia*) ones, promoted the development of larger pores, with greater specific surface areas. In contrast, the well-preserved, naturally elongated branched bryozoans, locally present in the *Fenestella*/*Kingopora* biofacies (an approximate equivalent of the bryozoan-foraminifer biofacies; cf. T. M. Peryt *et al*., 2012) significantly contributed to the formation of relatively narrow channel porosity. This probably favoured local improvements to permeability. It seems problematic, however, to find a well-preserved *Acanthocladia* anceps available for dissolution in the lowermost parts of Ca1. This results from increased energy of water, also noted by Fheed *et al*. (2015). Therefore, the moulds encountered in the Brońsko Reef show rather poor connectivity, although they have ensured a relatively high porosity.

CONCLUSIONS

It has been demonstrated that combining the sedimentological, diagenetic and petrophysical analyses is an efficient tool for the characterization of carbonate hydrocarbon reservoirs. The interpretation of well log and laboratory-derived petrophysical data, supported by diagenetic research, allowed the deciphering of the main factors that controlled reservoir quality. Sedimentological and microscope research, in turn, provided a thorough insight into distribution patterns of fossils and their contribution to the evolution of porosity. In addition, the μCT and NMR-derived data, discussed in other papers by the author, seem to complement the results obtained, particularly when pore geometry is considered.

The currently observed porosity and permeability show an evident dependence on the organisms that were fossilized as the site of mineralogically and microstructurally controlled dissolution. For instance, it was shown that a high degree of fragmentation of the *Acanthocladia* bryozoans, later dissolved to form mouldic porosity, lowered the permeability, with the simultaneous preservation of porosity. On the other hand, the channels created owing to the dissolution of foraminifer encrustations developed around the bryozoans, increased the permeability – particularly in the bryozoan-foraminifer biofacies. The latter seems to represent the best reservoir properties, resulting from the high variability of probably microstructurally deformed fossils and the presence of foraminifer encrustations, together having improved the efficiency of dissolution. The porosity of this horizon also was increased thanks to probable fresh-water flushing after deposition of the Ca1 strata, during which the bivalve-related caverns and intraparticle voids associated with bryozoans might have been formed.

The majority of caverns observed for the brachiopod-bryozoan and bivalve-gastropod biofacies, originated owing to the dissolution of the originally aragonitic bivalve and gastropod shells, and of terebratulid brachiopod coquinas. In the case of the latter biofacies, the dissolution probably took place partially during meteoric exposure, as deduced from numerous caverns, small-scale karren-like fractures and brecciation of rocks. Here, the impact of karst and further fresh-water flushing were probably responsible for a sound porosity-permeability correlation, also proved by similar PHIE (LLS) and helium porosity values, both being close to the total PHIT (D) porosity.

The two biofacies were the subject of intensive anhydrite cementation that occurred firstly during the sabkha conditions, as deduced from the widespread presence of chicken-wire anhydrite, and later, during shallow burial of the Ca1 strata (A1d brine seepage, and precipitation of lath-shaped anhydrite). Importantly, anhydrite cementation seems to have been the most severe factor reducing the porosity, which was reduced additionally by the crystallization of sparry, burial calcite.

Lastly, the higher porosity of the stromatolitic biofacies in the Brońsko-2 well probably resulted from the dolomitization, responsible for the evolution of vuggy porosity. However, the average permeability is dramatically low here, since the vugs are poorly interconnected. In general,

dolomitization occurred in several stages, including sabkha, reflux and burial realms.

The author believes that the conclusions gathered in this paper will help the evaluation of other, similar carbonate buildups in terms of joint petrophysical and sedimentological studies, so far uncommon for the Polish Ca1 strata, but generally common worldwide.

Acknowledgements

The work was funded by the Polish National Science Centre as Project No UMO-2016/23/N/ST10/00350 and by AGH University of Science and Technology, Faculty of Geology, Geophysics and Environmental Protection (Statutory Grant No 15.11.140.996). The author would like to thank the Polish Oil and Gas Company (PGNiG) for sharing well log and archival laboratory data (Agreement No OGiE/DW/DWA/000177/2016). Special thanks go to the reviewers Thilo Bechstädt, Reinhard Gaupp and Tadeusz Marek Peryt, for contributing to significant improvement in the quality of the paper. The author is also much indebted to Paweł Raczyński, for palaeontological support and to Anna Świerczewska for offering geological consultation. The feedback from Kamila Wawrzyniak-Guz on well log interpretation is also much appreciated.

REFERENCES

Abdioğlu, E., Arslan, M., Aydinçakir, D. & Gündoğan, I., 2015. Stratigraphy, mineralogy and depositional environment of the evaporite unit in the Aşkale (Erzurum) sub-basin, Eastern Anatolia (Turkey). *Journal of African Earth Sciences*, 111: 100–112.

Ahr, W. M., Allen, D., Boyd, A., Bachman, H. N., Clerke, F. A., Gzara, K. B. M., Hassall, J. K., Murty, C. R. K., Zubari, H. & Ramamoorthy, R., 2005. Confronting the carbonate conundrum. *Oilfield Review*, 17: 18–29.

Aleali, M., Rahimpour-Bonab, H., Moussavi-Harami, R. & Jahani, D., 2013. Environmental and sequence stratigraphic implications of anhydrite textures: A case from the Lower Triassic of the Central Persian Gulf. *Journal of Asian Earth Sciences*, 75: 110–125.

Anovitz, L. M. & Cole, D. R., 2015. Characterization and analysis of porosity and pore structures. *Reviews in Mineralogy and Geochemistry*, 80: 61–164.

Archie, G. E., 1942. Electrical resistivity log as an aid in determining some reservoir characteristics. *Transactions of the American Institute of Mining and Metallurgical Engineers*, 146: 54–67.

Asquith, G. & Krygowski, D., 2004. *Basic Well Log Analysis*. *AAPG Methods in Exploration, Series 16*. American Association of Petroleum Geologists, Tulsa, 248 pp.

Ballay, G., 2012. *The "m" Exponent in Carbonate Petrophysics*. http://www.geoneurale.com/documents/_m_Exponent.pdf, 18 pp. [15.05.2019].

Becker, F. & Bechstädt, T., 2006. Sequence stratigraphy of a carbonate-evaporite succession (Zechstein 1, Hessian Basin, Germany). *Sedimentology*, 53: 1083–1120.

Clark, D. B., 1986. The distribution of porosity in Zechstein carbonates. In: Brooks, J. C. & van Hoorn, B. (eds), *Habitat of Palaeozoic Gas in N. W. Europe.Geological Society Special Publication*, 23: 121–149.

Choquette, P. W. & James, N. P., 1988. Introduction. In: Choquette, P. W. & James, N. P. (eds), *Paleokarst.* Springer, New York, pp. 1–21.

Choquette, P. W. & Pray, L. C., 1970. Geological nomenclature and classification of porosity in sedimentary carbonates. *AAPG Bulletin*, 54: 207–250.

Crain, E. R., 1986. *The Log Analysis Handbook (Quantitative Log Analysis Methods)*. Pennwell Corp, Tulsa, 684 pp.

Demicco, R. V. & Hardie, L. A., 1994. *Sedimentary Structures and Early Diagenetic Features of Shallow Marine Carbonate Deposits*. SEPM Society for Sedimentary Geology, Tulsa, 272 pp.

Desrochers, A. & James, N. P., 1988. Early Paleozoic surface and subsurface paleokarst: Middle Ordovician Carbonates, Mingan Islands, Quebec. In: Choquette, P. W. & James, N. P. (eds), *Paleokarst.* Springer, New York, pp. 183–210.

Doornenbal, J. C., Abbink, O. A., Duin, E. J. T., Dusar, M., Hoth, P., Jasionowski, M., Lott, G. K., Mathiesen, A., Papiernik, B., Peryt, T. M., Veldkamp, J. G. & Wirth, H., 2010. Introduction, stratigraphic framework and mapping. In: Doornenbal, J. C. & Stevenson A. G. (eds), *Petroleum Geological Atlas of the Southern Permian Basin Area*. EAGE Publications b.v., Houten, pp. 1–9.

Dyjaczyński, K., Górski, M., Mamczur, S. & Peryt, T. M., 2001. Reefs in the basinal facies of the Ca1 (upper Permian) of western Poland: a new gas play. *Journal of Petroleum Geology*, 24: 265–285.

Dyjaczyński, K., Mamczur, S. & Radecki, S., 1997. New perspectives for gas deposits' prospection within the Zechstein Limestone strata, Foresudetic Monocline. *Przegląd Geologiczny*, 45: 1248–1256. [In Polish, with English summary.]

Eggie, L. A., Pietrus, E., Ramdoyal, A. & Chow, N., 2014. Diagenesis of the Lower Silurian Ekwan River and Attawapiskat formations, Hudson Bay Lowland, northern Manitoba (parts of NTS 54B, F, G). In: *Report of Activities, Manitoba Mineral Resources, Manitoba Geological Survey*, GS-14: 161–171.

Evamy, B. D., 1963. The application of a chemical staining technique to a study of dedolomitization. *Sedimentology*, 2: 164–170.

Fheed, A. & Krzyżak, A., 2017. A textural and diagenetic assessment of the Zechstein Limestone carbonates, Poland using the transverse Nuclear Magnetic Resonance relaxometry. *Journal of Petroleum Science and Engineering*, 152: 538–548.

Fheed, A. & Krzyżak, A., 2018. Diffusion-weighted nuclear magnetic resonance imaging (DWI) for fluid flow direction and intensity recognition in carbonates – examples from Permian reefs. In: *SEG/AAPG/EAGE/SPE Research and Development Petroleum Conference and Exhibition, RDP 2018, Abu Dhabi, May 9–10, 2018*. Society of Exploration Geophysicists Global Meeting Abstracts, pp. 140–143.

Fheed, A., Krzyżak, A. & Lalowicz, Z., 2017. Fossil-related porosity scanning by means of the nuclear magnetic resonance and computed microtomography – the Permian Bronsko Reef carbonates, Western Poland. In: *International Multidisciplinary Scientific Geoconference Surveying Geology and Mining Ecology Management, SGEM*, 17 (14), pp. 667–675.

Fheed, A., Krzyżak, A. & Świerczewska, A., 2018. Exploring a carbonate reef reservoir – nuclear magnetic resonance and computed microtomography confronted with narrow channel and fracture porosity. *Journal of Applied Geophysics*, 151: 343–358.

Fheed, A. & Strzelecki, P. J., 2017. *X-ray microtomography-based pore structure analysis of the Permian Reef rocks (West Poland)*. In: *International Multidisciplinary Scientific GeoConference Surveying Geology and Mining Ecology Management, SGEM*, 17 (15), pp. 661–667.

Fheed, A., Świerczewska, A. & Krzyżak, A., 2015. The isolated Wuchiapingian (Zechstein) Wielichowo Reef and its sedimentary and diagenetic evolution, SW Poland. *Geological Quarterly*, 59: 762–780.

Flügel, E., 2010. *Microfacies of Carbonate Rocks. 2nd Edition*. Springer, Berlin, 984 pp.

Frykman, P., Stentoft, N., Rasmussen, K. L., Christensen, O. W., Andersen, P. V. & Jacobsen, F. L., 1990. Diagenesis and porous system in Danish Zechstein carbonate reservoirs. *Geological Survey of Denmark*, 31: 1–107.

Fu, Q. & King, H., 2010. Medium and coarsely crystalline dolomites in the Middle Devonian Ratner Formation, southern Saskatchewan, Canada: Origin and pore evolution. *Carbonates and Evaporites*, 26: 111–125.

Füchtbauer, H., 1964. Facies, Porosität und Gasinhalt der Karbonatgesteine des norddeutschen Zechsteins. *Zeitschrift der Deutschen Geologischen Gesellschaft*, 114: 484–531.

Füchtbauer, H., 1980. Composition and diagenesis of a stromatolitic bryozoan bioherm in the Zechstein 1 (northwestern Germany). *Contributions to Sedimentology*, 9: 233–251.

Geluk, M. C., 2000. Late Permian (Zechstein) carbonate-facies maps, the Netherlands. *Netherlands Journal of Geoscience*, 79: 17–27.

Hara, U., Słowakiewicz, M. & Raczyński, P., 2013. Bryozoans (trepostomes and fenestrates) in the Zechstein Limestone (Wuchiapingian) of the North Sudetic Basin (SW Poland): palaeoecological implications. *Geological Quarterly*, 57: 417–432.

Harris, P. M., Kendall, C. G. & Lerche, I., 1985. Carbonate Cementation – a brief review. In: Schneidermann, N. & Harris, P. M. (eds), *Carbonate Cements. Society of Economic Paleontologists and Mineralogists Special Publication*, 36: 79–95.

Hollingworth, N. & Pettigrew, T., 1988. *Zechstein Reef Fossils and their Palaeoecology*. Palaeontological Association, University Printing House, Oxford, 75 pp.

Hollingworth, N. T. J. & Tucker, M. E., 1987. The Upper Permian (Zechstein) Tunstall Reef of North East England: Palaeoecology and early diagenesis. *Lecture Notes in Earth Sciences*, 10: 23–50.

Hu, X. & Huang, S., 2017. Physical properties of reservoir rocks. In: Xuetao, H., Shuyong, H., Fayang, J. & Huang, S. (eds), *Physics of Petroleum Reservoirs, Second Edition*. Springer Geophysics, Berlin, pp. 7–164.

Jasionowski, M., Durakiewicz, T. & Peryt, T. M., 2000. Rafy wapienia cechsztyńskiego (Ca1) na wyniesieniu wolsztyńskim w świetle badań stabilnych izotopów tlenu i węgla. *Przegląd Geologiczny*, 48: 468. [In Polish.]

Jasionowski, M., Peryt, T. M. & Durakiewicz, T., 2014. Polyphase dolomitisation of the Wuchiapingian Zechstein Limestone (Ca1) isolated reefs (Wolsztyn Palaeo-Ridge, Fore-Sudetic Monocline, SW Poland). *Geological Quarterly*, 58: 483–500.

Kaldi, J., 1986. Diagenesis of nearshore carbonate rocks in the Sprotbrough Member of the Cadeby (Magnesian Limestone) Formation (Upper Permian) of eastern England. In: Harwood, G. N. & Smith, D. B. (eds), *The English Zechstein and Related Topics*. *Geological Society Special Publication*, 22: 87–102.

Karaca, E., 2015. Pore structure and petrophysical characterization of Hamelin Pool stromatolites and pavements, Shark Bay, Western Australia. *Open Access Theses*, 567: 1–141.

Kerans, C. & Donaldson, J. A., 1988. Proterozoic paleokarst profile, Dismal Lakes Group, N.W.T. Canada. In: Choquette, P. W. & James, N. P. (eds), *Paleokarst.* Springer, New York, pp. 167–182.

Kerkmann, K., 1969. Riffe und Algenbänke im Zechstein von Thüringen. *Freiberger Forschungshefte*, C 252: 1–85.

Kiersnowski, H., Peryt, T. M., Buniak, A. & Mikołajewski, Z., 2010. From the intra-desert ridges to the marine carbonate island chain: middle to late Permian (Upper Rotliegend–Lower Zechstein) of the Wolsztyn-Pogorzela high, west Poland. *Geological Journal*, 45: 319–335.

Laongsakul, P. & Dürrast, H., 2011. Characterization of reservoir fractures using conventional geophysical logging. *Songklanakarin Journal of Science and Technology*, 33: 237–246.

Luthi, S. M., 2013. *Geological Well Logs: Their Use in Reservoir Modeling*. Springer Science & Business Media, Berlin, 373 pp.

Machel, H. G., 2004. Concepts and models of dolomitization: a critical reappraisal. In: Braithwaite, C. J. R., Rizzi, G. & Darke, G. (eds), *The Geometry and Petrogenesis of Dolomite Hydrocarbon Reservoirs*. *Geological Society Special Publication*, 235: 7–63.

Machel, H. G. & Burton, E. A., 1991. Burial-diagenetic sabkha-like gypsum and anhydrite nodules. *Journal of Sedimentary Petrology*, 61: 394–405.

Mazzullo, S. J., 2004. Overview of porosity evolution in carbonate reservoirs. *Kansas Geological Society Bulletin*, 79: 22–27.

Mikołajewski, Z., Buniak, A. & Chmielowiec-Stawska, A., 2009. Charakterystyka właściwości zbiornikowych w rafowych utworach wapienia cechsztyńskiego (Ca1) na przykładzie złoża Brońsko. *Przegląd Geologiczny*, 57: 309–310. [In Polish.]

Moore, C. H., 1989. Carbonate diagenesis and porosity. In: Moore, C. H. (ed.), *Introduction to Diagenesis in the Meteoric Environment, VI. Developments in Sedimentology*, 46: 161–175.

Moore, C. H. & Wade, W. J., 2013. Carbonate reservoirs: porosity and diagenesis in a sequence stratigraphic framework. In: Moore, C. H. & Wade, W. J. (eds), *Carbonate Diagenesis: Introduction and Tools, V. Developments in Sedimentology*, 67: 67-89.

Nollet, S., Hilgers, C. & Urai, J., 2005. Sealing of fluid pathways in overpressure cells: a case study from the Buntsandstein in the Lower Saxony Basin (NW Germany). *International Journal of Earth Sciences*, 94: 1039–1055.

Nusara, S., Punya, C., Sarunya, P. & Ken-Ichiro, H., 2017. Petrology and alteration of calcium sulphate deposits in late Paleozoic rocks of Wang Saphung area, Loei province, Thailand. *Journal of Earth Science and Climatic Change*, 8: 384.

Paul, J., 1980. Upper Permian algal stromatolite reefs, Harz Mountains (F.R. Germany). *Contributions to Sedimentology*, 9: 253–268.

Paul, J., 2010. Zechstein reefs in Germany. In: Doornenbal, J. C. & Stevenson, A. G. (eds), *Petroleum Geological Atlas of the Southern Permian Basin Area*. EAGE Publications b.v., Houten, pp. 142–144.

Peryt, D., Peryt, T. M., Raczyński, P. & Chłódek, K., 2012. Foraminiferal colonization related to the Zechstein (Lopingian)

transgression in the western part of the Wolsztyn Palaeo-Ridge area, Western Poland. *Geological Quarterly*, 56: 529–546.

Peryt, T. M., 1984. Sedimentation and early diagenesis of the Zechstein Limestone in Western Poland. *Prace Instytutu Geologicznego*, 109: 1–80. [In Polish, with English summary.]

Peryt, T. M. & Peryt, D., 2012. Geochemical and foraminiferal records of environmental changes during Zechstein Limestone (Lopingian) deposition in northern Poland. *Geological Quarterly*, 56: 187–198.

Peryt, T. M., Raczyński, P., Peryt, D. & Chłódek, K., 2012. Upper Permian reef complex in the basinal facies of the Zechstein Limestone (Ca1), western Poland. *Geological Journal*, 47: 537–552.

Peryt, T. M., Raczyński, P., Peryt, D., Chłódek, K. & Mikołajewski, Z., 2016. Sedimentary history and biota of the Zechstein Limestone (Permian, Wuchiapingian) of the Jabłonna Reef in western Poland. *Annales Societatis Geologorum Poloniae*, 86: 379–413.

Pharaoh, T. C., Dusar, M., Geluk, M., Kockel, F., Krawczyk, C., Krzywiec, P., Schneck-Wenderoth, M., Thybo, H., Vejbaek, O. & Wees, J.-D. van, 2010. Tectonic evolution. In: *Petroleum Geological Atlas of the Southern Permian Basin Area*, EAGE Publications b.v., Houten, pp. 25–58.

Pikulski, L. & Wolnowski, T., 2005. Geological Analysis of the Zechstein Limestone Formations (Ca1) in Western Poland. In: *AAPG Search and Discovery. AAPG/EAGE International*. *Research Conference, El Paso, Texas, October 1–5*, *2005*, p. 50.

Raczyński, P., 2000. Zespoły organizmów w kompleksie rafowym wapienia cechsztyńskiego (Ca1) na wyniesieniu wolsztyńskim. *Przegląd Geologiczny*, 48: 469–470. [In Polish.]

Raczyński, P., Peryt, T. M., Peryt, D., 2016. Sedimentary history of two Zechstein Limestone carbonate buildups (Elżbieciny and Racot) in western Poland: the reefs that were. *Zeitschrift der Deutschen Gesellschaft für Geowissenschaften*, 167: 191–210.

Raczyński, P., Peryt, T. M. & Strobel, W., 2017. Sedimentary and environmental history of the Late Permian Bonikowo Reef (Zechstein Limestone, Wuchiapingian), western Poland. *Journal of Palaeogeography*, 6: 183–205.

Reijers, T. J. A., 2012. Sedimentology and diagenesis as 'hydrocarbon exploration tools' in the Late Permian Zechstein-2 Carbonate Member (NE Netherlands). *Geologos*, 18: 163–195.

Roshnan, H., Sari, M., Arandiyan, H., Hu, Y., Mostaghimi, P., Sarmadivaleh, M., Masoumi, H., Veveakis, M., Iglauer, S. & Regenauer-Lieb, K., 2019. Total porosity of tight rocks: a welcome to the heat transfer technique. *Energy Fuels, American Chemical Society*, 30: 10072–10079.

Schlumberger, 1989. *Log Interpretation Principles/Applications*. Schlumberger Wireline & Testing, c1991, Houston, Texas, 241 pp.

Schlumberger, 2014. *Techlog 2014: User's Manual*. Schlumberger Limited, Houston.

Scholle, P. A. & Ulmer-Scholle, D. S., 2003. *A Colour Guide to the Petrography of Carbonate Rocks: Grains, Textures, Porosity, Diagenesis*. *AAPG Memoir*, 77: 1–474.

Schön, J., 2015. *Basic Well Logging and Formation Evaluation:* Bookboon.com, London, 179 pp.

Smith, D. B., 1970. Submarine slumping and sliding in the lower Magnesian Limestone of Northumberland and Durham. *Proceedings of the Yorkshire Geological Society*, 38: 1–36.

Smith, D. B., 1972. Foundered strata, collapse-breccias and subsidence features of the English Zechstein. In: *Geology of Saline Deposits: Proceedings of the Hannover Symposium*. UNESCO, Paris, pp. 255–269.

Smith, D. B., 1980. The evolution of the English Zechstein basin. *Contributions to Sedimentology*, 9: 7–34.

Smith, D. B., 1986. The Trow Point Bed–a deposit of Upper Permian marine oncoids, peloids and columnar stromatolites in the Zechstein of NE England. In: Harwood, G. M. & Smith, D. B. (eds), *The English Zechstein and Related Topics*. *Geological Society Special Publication*, 22: 113–125.

Smith, D. B., 1995. *Marine Permian of England*. Geological Conservation Review Series, Chapman and Hall, 8, London, 205 pp.

Stanley, G. D., 2001. Introduction to reef ecosystems and their evolution. In: Stanley, G. D. (ed.), *The History and Sedimentology of Ancient Reef Systems*. Springer Science & Business Media, New York, pp. 1–40.

Steinhoff, I. & Strohmenger, C., 1996. Zechstein 2 carbonate platform subfacies and grain-type distribution (Upper Permian, Northwest Germany). *Facies*, 35: 105–132.

Taylor, P. D. & Wilson, M. A., 2003. Palaeoecology and evolution of marine hard substrate communities. *Earth-Science Reviews*, 62: 1–103.

Tucker, M. E. & Wright, V. P., 1990. *Carbonate Sedimentology*. Blackwell Science, Oxford, 482 pp.

Van Der Baan, D., 1990. Zechstein reservoirs in the Netherlands. In: Brooks, J. (ed.), *Classic Petroleum Provinces. Geological Society Special Publication*, 50: 379–398.

Walter, L. M., 1985. Relative reactivity of skeletal carbonates during dissolution: implications for diagenesis. In: Schneidermann, N. & Harris, P. M. (eds), *Carbonate Cements*. *Society of Economic Paleontologists and Mineralogists Special Publications*, 36: 3–16.

Warren, J. K., 2016. *Evaporites: A Geological Compendium.* Springer, Berlin, 1854 pp.

Weidlich, O., 2002. Middle and Late Permian reefs – distributional patterns and reservoir potential. In: Kiessling, W., Flügel, E. & Golonka, J. (eds), *Phanerozoic Reef Patterns. SEPM Society for Sedimentary Geology Special Publication,* 72: 339–390.

Wyllie, M. R. J., Gregory, A. R. & Gardner, G. H. F., 1958. An experimental investigation of factors affecting elastic wave velocities in porous media. *Geophysics*, 23: 459–493.

Appendix

Compilation of petrophysical (He: Helium porosity; PHIE LLS: shallow resistivity effective porosity; N_2: nitrogen permeability) and microscope (pore geometry, thin section description) data. Biofacies are abbreviated according to Figures 2 and 3, whereas lithofacies given in brackets correspond to those from Table 1. Bold values denote average porosity/permeability. The first row of the average values corresponds to the data limited to the corresponding depths for thin sections. The second row of the average values (bold italics) represents the whole datasets available, and the number of observations is specified in brackets

Brońsko-1								
Sample No.	**Extraction depth [m]**		**Bio- and lithofacies**	**He poros. [%]**	**PHIE LLS [%]**	**N_2 perm. [mD]**	**Main geometric pore types (thin sections)**	**Microscope observations**
	Thin section	**Plug sample**						
AM2	2196.63	2197.05	S (B)	9.13	8.68	2.45	Fracture Channel Single moulds	Numerous laminae, stromatolites.
AR3/ AM5	2200.78	2201.00	S (P/R)	16.68	17.63	33.88	Channel Vug	Extremely abundant foraminifer-related channels.
				12.9	**13.16**	**18.17**		
				9.24 (10)	***9.10 (50)***	***20.17 (10)***		
AM9	2203.32	2203.00	BF (P/R)	13.63	18.35	2.89	Vug Mouldic	Components commonly larger than 2 mm.
AR5/ AM8	2202.09	2202.15	BF (P/R)	16.46	12.17	58.89	Mouldic Channel Intraparticle Intercrystal.	Numerous fenestral/columnar bryozoans, ostracods. Common anhydrite. Sparry and prismatic calcite. Foraminifer-related channels.
AR7/ AM10	2204.34	2204.50	BF (P/R)	23.24	18.63	55.84	Cavernous Vug Channel	Large caverns, drusy calcite, sparry, poikilotopic and rosette anhydrite, limited amount of foraminifer-related channels. Single, sharp-ended lenticular gypsum crystals (?).
AR9/ AM12	2206.12	2206.45	BF (P/R)	6.66	7.41	3.17	Channel Mouldic Intraparticle	Numerous channels along branched bryozoans, muddy intercalations.
AR10/ AM13	2207.24	2207.75	BF (P/R)	10.82	18.32	0.01	Mouldic Intraparticle Channel Fracture Vug	A lot of dissolved foraminifer and gastropod shells.
AR12/ AM14	2209.13	2209.00	BF (P/R)	17.22	21.85	40.17	Mouldic Intercrystal. Intraparticle	Intensive dolomitization (dolomicrite) and dolomite cementation (isopachous dolomite). Sparry, poikilotopic anhydrite is common.
AM15	2210.43	2210.60	BF (P/R D-)	15.69	19.98	68.42	Mouldic Intraparticle Interparticle Vug Channel	A lot of sparry calcite. High carbonate mud content. Numerous bivalves and bryozoans.

Brońsko-1								
Sample No.	**Extraction depth [m]**		**Bio- and lithofacies**	**He poros. [%]**	**PHIE LLS [%]**	**N_2 perm. [mD]**	**Main geometric pore types (thin sections)**	**Microscope observations**
	Thin section	**Plug sample**						
AR14	2213.19	2213.50	BF (P/R D-)	11.43 **14.39** ***13.74 (23)***	9.71 **15.80** ***16.01 (128)***	2.37 **32.66** ***23.04 (23)***	Channel Mouldic	Dense foraminifer-related channel network. Sparry calcite and anhydrite fill the pore spaces.
AM17	2214.15	2214.10	BB (P/R D-)	15.17	15.63	0.69	Vug Mouldic Intercrystal. Intraparticle Channel	Dolomitization (several stages), sulphate cementation (sparry and chicken-wire anhydrite are common).
AR15	2218.85	2219.00	BB (P/R D-)	4.68	10.99	0.66	Fracture Vug Mouldic Intercrystal.	Numerous brachiopod shells cemented either with sparry calcite or rosette/chicken-wire anhydrite. Medium-crystalline dolosparite is common.
AR16/ AM20	2219.95	2220.00	BB (P/R D-)	3.58 **7.81** ***11.79 (12)***	7.34 **11.32** ***13.11 (66)***	0.01 **0.45** ***23.67 (12)***	Intercrystal. Fracture Intraparticle	Texture obliteration due to dolomitization. "Ghosts" of ostracods and bivalves are present.
AR17	2222.84	2222.50	BG (DP/R)	12.49	8.68	7.66	Vug Channel Fracture	Intensive cementation. Two or more stages of dolomization. Sulphate cementation (lath-shaped anhydrite and poikilotopic anhydrite cement). Horizontal stylolites cutting the anhydrite crystals commonly occur. Wide channels – up to 0.7 mm.
AR19/ AM24	2226.07	2226.00	BG (P/R D-)	5.92	5.51	0.02	Intercrystal. Mouldic	Complete texture obliteration due to dolomitization (several episodes). Widespread anhydrite cementation (both rosette-like and pile-of-bricks fabrics). Dolomicrite inclusions within the anhydrite crystals.
AR20/ AM26	2228.24	2228.50	BG (DP/G)	18.90 **12.44** ***13.86 (21)***	19.01 **11.06** ***12.78 (118)***	0.93 **3.84** ***21.36 (21)***	Fracture Intercrystal. Single moulds	Common lath-shaped anhydrite crystals. Single moulds after ostracods. Multistage dolomitization. The rock has a tight, highly dolomitized matrix.
AR22/ AM28	2232.86	2233.00	A (DP/G)	8.09	13.80	0.23	Cavernous Intercrystal. Intraparticle	Widespread sparry, poikilotopic and lath-shaped anhydrite. Isopachous dolomite cement surrounding the terebratulid brachiopod shells with primary intraparticle porosity preserved.
AR24/ AM30	2238.25	2238.00	A (DG)	25.27	31.00	10.91	Intraparticle Intercrystal.	Numerous terebratulid brachiopod shells. Sparry anhydrite and medium-crystalline dolosparite are common. Branched bryozoans often occur.

Sample No.	Extraction depth [m]		Bio- and lithofacies	He poros. [%]	PHIE LLS [%]	N_2 perm. [mD]	Main geometric pore types (thin sections)	Microscope observations
	Thin section	Plug sample						
Brońsko-1								
AM31	2240.30	2240.50	A (DG)	26.60	18.28	10.76	Intraparticle Intercrystal.	Numerous branched and columnar bryozoans with intraparticle porosity. Crystal fabrics as for AR24. Growing proportion of crinoids.
AR26/ AM33	2241.70	2241.50	A (DG)	14.90	19.21	64.69	Fracture	Common Carboniferous extraclasts containing quartz and clay minerals. Fragmented branched bryozoans. Carbonate breccia cut by fractures and horizontal stylolites are present.
AM34	2245.85	2246.05	A (DG)	11.38	16.81	0.29	Intraparticle Poorly developed intercrystal. Mouldic	Numerous bivalve shells surrounded by isopachous, prismatic calcite. Subordinate dolomitization.
				17.25	**19.82**	**21.65**		
				17.26 (31)	***18.22 (156)***	***16.50 (31)***		
Brońsko-2								
BM1	2182.48	2182.55	S (B)	16.07	17.73	0.31	Vuggy Fenestral? Intercrystal.	Stromatolites, sparry anhydrite, dolomitization. Dolomite cement forms isopachous rims around the grains. Numerous gastropods are present.
BM2	2183.50	2183.55	S (B)	17.49	14.40	0.01	Vuggy Intercrystal.	Stromatolites, chicken-wire anhydrite, dolomitization and synsedimentary fractures filled with calcite (currently representing veins).
				16.78	**16.07**	**0.16**		
				10.80 (8)	***14.21 (35)***	***0.15 (8)***		
BR2	2185.65	2186.00	BG (PGA)	5.02	2.14	0.01	Poorly developed intercrystal.	Stromatolites and brachiopod shells cemented with sparry, poikilotopic anhydrite. Single fractures are also cemented with anhydrite.
BR3	2186.88	2187.10	BG (PGA)	0.33	8.27	0.01	Mouldic Vuggy Channel	Numerous dissolved shells of foraminifers, ostracods and gastropods, distributed among a dense bryozoan-related mouldic porosity network. Sparry calcite and anhydrite fill the pore spaces.
BR4/ BM6	2188.40	2188.55	BG (P/G)	10.81	15.03	5.89	Intraparticle Mouldic Channel Fracture	Dissolved bryozoan zoaria co-occurring with moulds after foraminifers, ostracods and bivalves. Large cavities are cemented with sparry calcite (veins). Ferroan oxides and barite (mainly artificial, coming from drilling mud) are present.
BR5	2191.90	2192.00	BG (P/G)	11.43	13.26	4.43	Channel Intraparticle	Numerous foraminifer-related channels. Intraparticle, bryozoan-related pores are common as well.

Brońsko-2								
Sample No.	**Extraction depth [m]**		**Bio- and lithofacies**	**He poros. [%]**	**PHIE LLS [%]**	**N_2 perm. [mD]**	**Main geometric pore types (thin sections)**	**Microscope observations**
	Thin section	**Plug sample**						
BM11	2193.41	2193.50	BG (P/G)	23.02	20.56	53.9	Well-developed intraparticle Mouldic	Partially dolomitized packstone with numerous columnar bryozoans (containing intraparticle voids), foraminifers, gastropods (moulds and intraparticle pores), bivalves with dolomitized margins (dolosparite), and single ostracods. Chicken-wire anhydrite and sparry, burial calcite are common. Marine, fibrous calcite is present as well.
BR8	2196.08	2196.00	BG (DG/DW)	15.72	21.96	0.66	Mouldic Intraparticle Intercrystal.	Dolograinstone with moulds and intraparticle pores after gastropods, bryozoans and bivalves. Isopachous dolomite cement rims the bioclasts. Chicken-wire anhydrite fills larger cavities. Prismatic structure of the bivalve shells.
				11.05	**13.54**	**10.82**		
				14.92 (23)	***16.07 (115)***	***23.83 (23)***		
BM14	2198.38	2198.50	A (DG/DW)	14.62	18.81	1.96	Mouldic Intraparticle Intercrystal. Vug	The rock is dolomitized and cemented with dolomite (clear isopachous rims of dolomite surrounding the bioclasts). Limited anhydrite cementation (typically sparry or lath-shaped). Numerous branched bryozoans are present. Single ostracods and gastropods occur.
BR10	2200.15	2200.00	A (G)	20	7.7	14.1	Mouldic Intraparticle Intercrystal. Vug	Medium-crystalline dolosparite is widespread. Clear intraparticle pores within the bryozoan zoaria. Limited amounts of sparry, lath-shaped and poikilotopic anhydrite cements.
				17.31	**13.26**	**8.03**		
				12.44 (8)	***12.89 (35)***	***4.02 (8)***		